

AWARD NUMBER: W81XWH-15-1-0277

TITLE: ERF is a Potential ERK-Modulated Tumor Suppressor in Prostate Cancer

PRINCIPAL INVESTIGATOR: Dr. Rohit Bose

CONTRACTING ORGANIZATION: Sloan Kettering Institute for Cancer Research
New York NY 10065

REPORT DATE: October 2017

TYPE OF REPORT: Annual

PREPARED FOR: U.S. Army Medical Research and Materiel Command
Fort Detrick, Maryland 21702-5012

DISTRIBUTION STATEMENT: Approved for Public Release;
Distribution Unlimited

The views, opinions and/or findings contained in this report are those of the author(s) and should not be construed as an official Department of the Army position, policy or decision unless so designated by other documentation.

REPORT DOCUMENTATION PAGE				Form Approved OMB No. 0704-0188	
Public reporting burden for this collection of information is estimated to average 1 hour per response, including the time for reviewing instructions, searching existing data sources, gathering and maintaining the data needed, and completing and reviewing this collection of information. Send comments regarding this burden estimate or any other aspect of this collection of information, including suggestions for reducing this burden to Department of Defense, Washington Headquarters Services, Directorate for Information Operations and Reports (0704-0188), 1215 Jefferson Davis Highway, Suite 1204, Arlington, VA 22202-4302. Respondents should be aware that notwithstanding any other provision of law, no person shall be subject to any penalty for failing to comply with a collection of information if it does not display a currently valid OMB control number. PLEASE DO NOT RETURN YOUR FORM TO THE ABOVE ADDRESS.					
1. REPORT DATE October 2017		2. REPORT TYPE Annual		3. DATES COVERED 30 Sep 2016 - 29 Sep 2017	
4. TITLE AND SUBTITLE ERF is a Potential ERK-Modulated Tumor Suppressor in Prostate Cancer				5a. CONTRACT NUMBER	
				5b. GRANT NUMBER W81XWH-15-1-0277	
				5c. PROGRAM ELEMENT NUMBER	
6. AUTHOR(S) Rohit Bose E-Mail: Boser@mskcc.org				5d. PROJECT NUMBER	
				5e. TASK NUMBER	
				5f. WORK UNIT NUMBER	
7. PERFORMING ORGANIZATION NAME(S) AND ADDRESS(ES) Sloan Kettering Institute for Cancer Research 1275 York Avenue New York NY 10065-6007				8. PERFORMING ORGANIZATION REPORT NUMBER	
9. SPONSORING / MONITORING AGENCY NAME(S) AND ADDRESS(ES) U.S. Army Medical Research and Materiel Command Fort Detrick, Maryland 21702-5012				10. SPONSOR/MONITOR'S ACRONYM(S)	
				11. SPONSOR/MONITOR'S REPORT NUMBER(S)	
12. DISTRIBUTION / AVAILABILITY STATEMENT Approved for Public Release; Distribution Unlimited					
13. SUPPLEMENTARY NOTES					
14. ABSTRACT Half of all prostate cancers contain an oncogenic gene fusion between the androgen-regulated upstream elements of the TMPRSS2-gene with the consequently upregulated ETS transcription factor ERG. Despite this high prevalence, detecting the presence of TMPRSS2-ERG in patients' tumors has little-to-no useful clinical utility, in part due to a lack of understanding of its mechanisms of oncogenesis. I have characterized a gene, ERF, which functions as a putative tumor suppressor. I had hypothesized that ERF is outcompeted by the TMPRSS2-ERG gene product. Currently, I have identified how ERF and ERG may compete with each other, and as a result, have opposing effects on cancer cell proliferation. I am currently now investigating the tumor suppressor function of ERF in prostate cancers lacking TMPRSS2-ERG.					
15. SUBJECT TERMS prostate cancer, tumor suppressor, TMPRSS2-ERG					
16. SECURITY CLASSIFICATION OF:			17. LIMITATION OF ABSTRACT	18. NUMBER OF PAGES	19a. NAME OF RESPONSIBLE PERSON
a. REPORT	b. ABSTRACT	c. THIS PAGE			USAMRMC
U	U	U	UU	35	19b. TELEPHONE NUMBER (include area code)

Table of Contents

	<u>Page</u>
1. Introduction.....	4
2. Keywords.....	4
3. Accomplishments.....	5
4. Impact.....	16
5. Changes/Problems.....	16
6. Products.....	17
7. Participants & Other Collaborating Organizations.....	18
8. Special Reporting Requirements.....	18
9. Appendices.....	19

ERF IS A POTENTIAL ERK-MODULATED TUMOR SUPPRESSOR IN PROSTATE CANCER

INTRODUCTION

Metastatic prostate cancer is the second most frequent cause of cancer death among American men and remains incurable. Half of such cancers contain a gene fusion, placing a slightly truncated ERG transcription factor downstream of the androgen-regulated promoter of TMPRSS2. This leads to significant upregulation of ERG, which drives tumorigenesis. ERG belongs to the ETS family of transcription factors, which contain the highly conserved ETS DNA-binding domain. There are differences in the biology of fusion-positive tumors versus those lacking the ERG fusion (fusion-negative). However, there is no targeted clinical strategy for treating either fusion-positive or fusion-negative cancers. This is partly due to our limited understanding of how exactly ERG promotes oncogenesis, as well as a lack of awareness of complimentary pathways in fusion-negative tumors. A recent multi-institutional effort sequencing metastatic prostate cancers yielded ERF as 1 of only 19 genes achieving the highest statistical criteria for containing cancer-relevant mutations, with several frameshift mutations as well as point mutations of key conserved residues noted in the critical ETS domain, presumably corresponding to loss-of-function mutations. ERF has known tumor suppressor ability and belongs to the same transcription factor family as ERG, contains a virtually identical DNA-binding ETS domain, but is a strong transcriptional repressor unlike the transcriptionally activating ERG. Most interestingly, all tumors with ERF mutations were fusion-negative. We hypothesize that in fusion-negative tumors, ERF functions as a tumor suppressor by occupying ETS binding sites and inhibiting gene expression, consistent with its repressor function. On the other hand, in fusion-positive tumors, loss of ERF function confers no discernible growth advantage, since ERF is already outcompeted at ETS binding sites by the upregulated ERG oncogene, which in turn activates gene transcription.

KEYWORDS

prostate cancer, tumor suppressor, TMPRSS2-ERG

ACCOMPLISHMENTS

Goals and Accomplishments

I. Specific Aim 1: To investigate how ERF and ERG may compete and have opposing effects on cancer cell proliferation

A. Major Task 1: Evaluate role of ERF in negatively regulating ERG-dependent genes

Nothing to report (please see 2016 annual report for previous data).

B. Major Task 2: Evaluate role of ERF in competing for DNA binding with ERG

Last year, I described the development and analysis of a VCaP-based system to study competition between ERG and ERF binding for chromatin. These are two ETS transcription factors that have a similar DNA-binding motif but have intrinsically positive or negative transcriptional activity, respectively. The VCaP system was ideal for initial studies, since it has high levels of endogenous ERG. However, this left open the possibility that the competition that we observed was a cell-line specific phenomenon, and not generalizable to other prostate cancers or normal prostate tissue.

To this end, and given the role that ERF also plays in benign prostate cells, I performed ChIP-seq to confirm that ERF binds ETS sites in normal prostate organoids. It is important to note that ERG is not endogenously expressed in normal prostate, unlike half of prostate cancers (Fig. 1a). De novo motif analysis of the ERF ChIP-seq peaks identified the canonical GGAA ETS DNA motif as the primary ERF binding site (Fig. 1e). Remarkably, transient overexpression of ERG led to a significant decrease of ERF chromatin occupancy (Fig. 1a-e), consistent with the competition for binding also seen previously in VCaP cancer cells. Furthermore, the ChIP-seq signal intensity of the smaller number of ERF peaks observed in the FLAG-ERG state was increased in the FLAG-alone state in almost all cases (Fig. 1b). Sh3bp5 and Rph3a1 are example genes demonstrating the ERG-mediated inhibition of ERF chromatin occupancy (Fig. 1d). Given the similarity of the ETS domains between ERF and ERG, as well as the ability of ETS factors to displace one another from canonical GGAA motifs, we postulated that the opposing effects of ERF and ERG could be explained by competition for ETS binding sites. I explored the overlap between androgen receptor and ERF sites in normal prostate organoids by androgen receptor ChIP-seq and found 28% of the ERF sites overlap with androgen receptor binding sites (Fig. 1e). This was lower than observed in the previously analyzed ERG-positive VCaP tumor cells, consistent with differences in androgen receptor chromatin occupancy between normal prostate and cancer. Collectively, these data suggest a model whereby the relative levels of ERF and ERG compete for ETS binding sites.

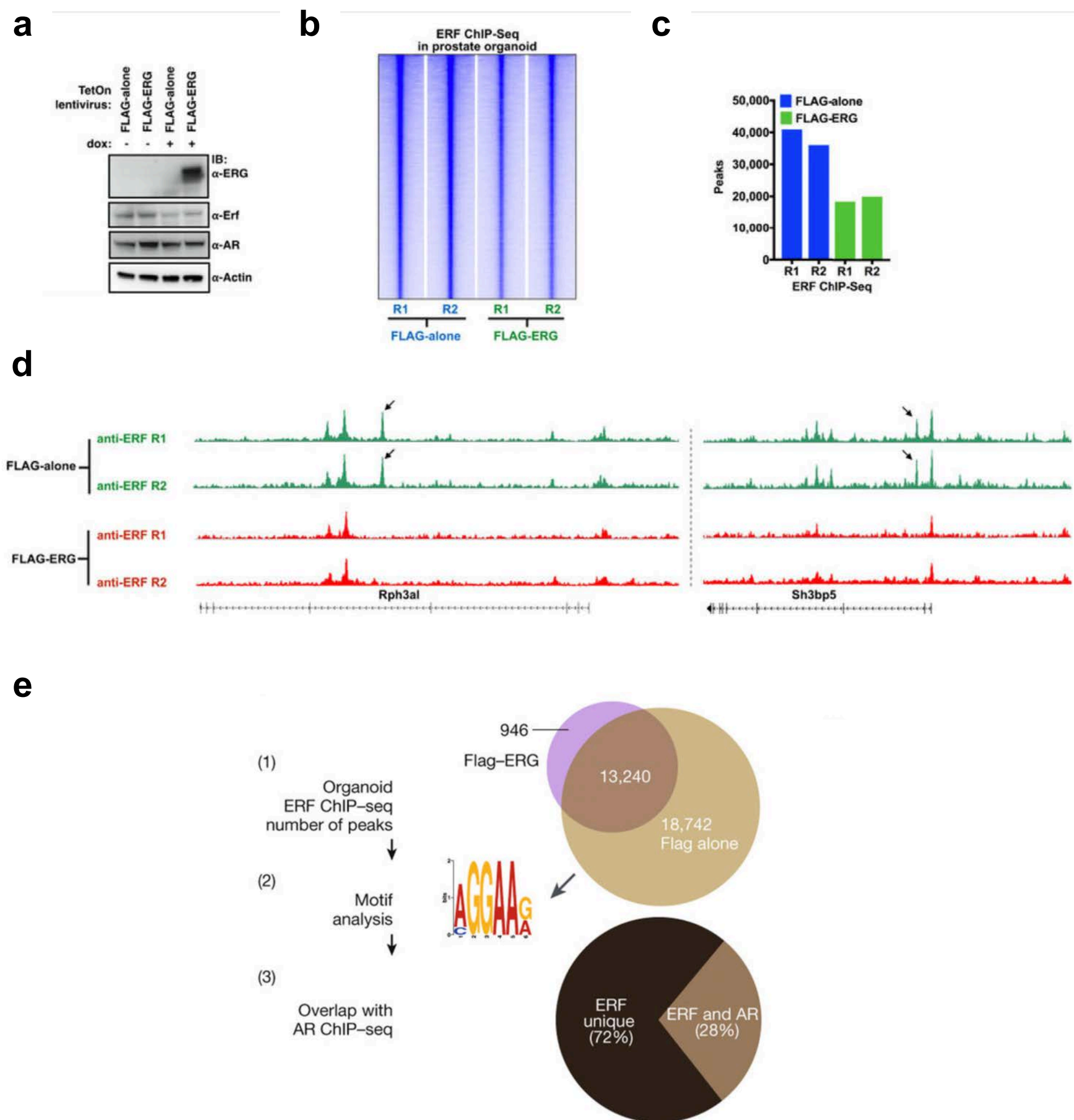


Figure 1 - a) Mouse normal prostate organoids were infected with a TetOn doxycycline-inducible Flag-ERG or empty vector (Flag-alone) and treated with or without doxycycline. **b)** ERF ChIP-seq in normal prostate organoids infected with either Flag-alone or Flag-ERG lentivirus, both treated with doxycycline (n = 2 biological replicates: R1, R2), and analysed with heat maps. **c)** Comparison of ERF ChIP-seq peak numbers, n = 2 biological replicates (R1, R2). **d)** ERF ChIP-seq signals for example genes Rph3a1 and Sh3bp5 loci, normalized by read depths. **e)** ERF ChIP-seq in normal prostate organoids infected with either a Flag-ERG lentivirus or Flag alone, both treated with doxycycline (n = 2 biological replicates: R1, R2) analysed by (1) peak overlap, (2) motif analysis, and (3) overlap with ERG and androgen receptor ChIP-seq.

C. Major Task 3: Evaluate for in vitro role of shERF

The near complete lack of ERF mutations in tumors with TMPRSS2–ERG fusions led us to investigate whether ERF loss recapitulates the phenotype of ERG gain, keeping in mind that ERG is not expressed in benign prostate epithelium. Last year, I described the development and analysis of normal murine prostate organoids with ERF knockdown. However, ERG only displays potent oncogenicity in a mouse *Pten*^{-/-} background. To this end, and to determine whether ERF loss yields a phenotype similar to ERG gain, I now infected prostate organoids derived from *Pten*^{-/-} mice with short hairpin RNA (shRNA) targeting mouse Erf (shErf_m). The *Pten*^{-/-} shErf_m organoids acquired morphological characteristics of ERG overexpression: they formed luminal structures lacking basal cells (Fig. 2a), and profiling by RNA sequencing (RNA-seq) and qPCR demonstrated profound loss of expression of most basal signature genes (Fig. 2b–e). Consistent with these changes, RNA-seq profiling revealed significant enrichment for genes whose expression is upregulated by androgen in human prostate cancer cells (Fig. 2c - right panel), which will be explored further in Specific Aim 3. Collectively, this supports the hypothesis that ERF loss leads to a pro-luminal shift, consistent with the changes observed as normal prostate tissue transitions to adenocarcinoma.

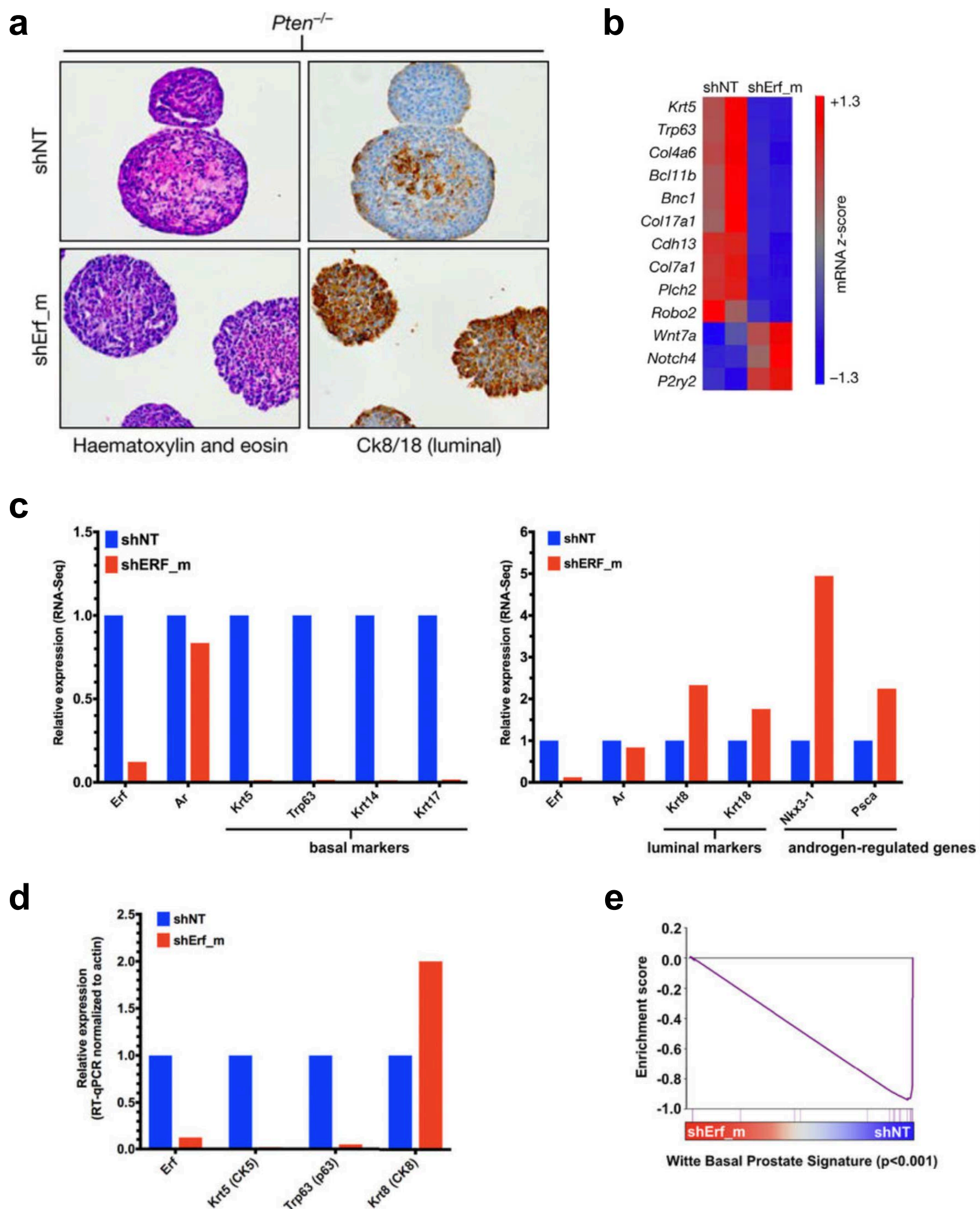


Figure 2 - a) Immunohistochemistry of *Pten*^{-/-} mouse prostate organoids infected with non-targeting shRNA (shNT) or targeting ERF (shErf_m). **b)** Basal signature applied to *Pten*^{+/+} organoid RNA-seq (n = 2 biological replicates). **c)** RNA-seq analysis of organoids derived from *Pten*^{+/+} and *Pten*^{-/-} mouse prostates infected with non-targeting shNT or shErf_m; n = 2 biological replicates. **d)** RT-qPCR analysis of the *Pten*^{+/+} organoids; n = 2 biological replicates. **e)** *Pten*^{+/+} organoid RNA-seq (n = 2 biological replicates) interrogated by GSEA for expression signature of Witte basal prostate cancer

Specific Aim 2: To evaluate for in vivo tumor suppressor function of ERF

A. Major Task 1: Evaluate role of ERF as in vivo tumor suppressor

The *Pten*^{-/-} organoids infected with shErf_m were indeed able to form tumors when grafted back into mice, recapitulating the phenotype of ERG overexpression and confirming that ERF is a bona fide tumor suppressor (Fig. 3a). Next, to assess the impact of ERF in human prostate cancers, we interrogated the mRNA expression profiles of the primary and metastatic human prostate cohorts TCGA-333 and SU2C-150 respectively. In agreement with the prior functional studies, ERF mRNA levels are inversely correlated with two luminal transcriptional activity signatures both in normal human prostate and in all primary tumor subtypes (Fig. 3b). This reciprocal association is also observed in metastatic cancers if the analysis is limited to tumors without amplification of or mutations in the AR gene, which encodes the androgen receptor (Fig. 3c). The fact that reduced ERF expression enhances luminal transcriptional output even in the absence of mutation or deletion, raises the possibility that ERF may have a broader role in prostate oncogenesis.

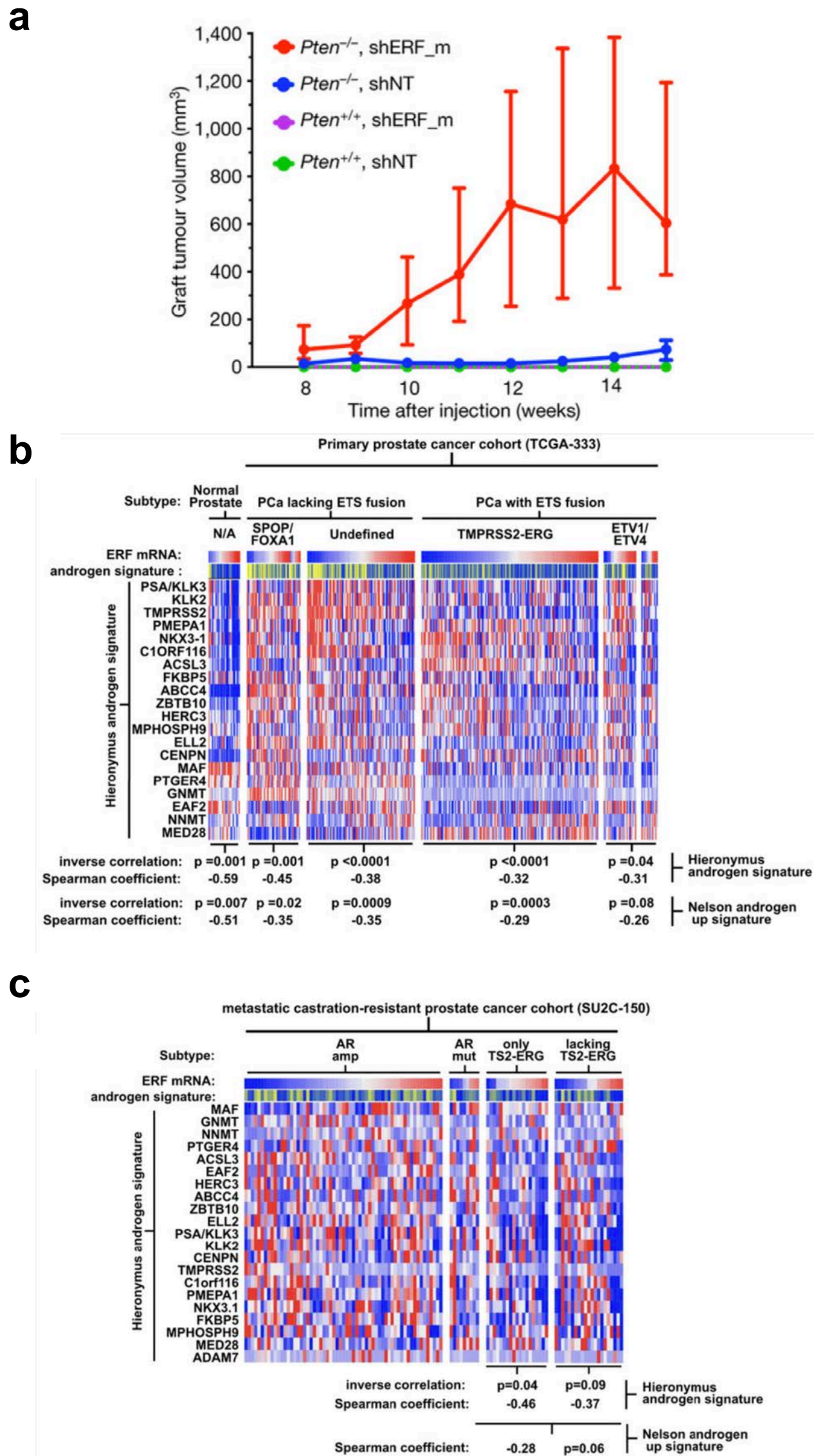


Figure 3 - a) Graft tumour volumes of GEMM-derived prostate organoids. Data are median \pm interquartile range; $n = 10$ tumours per condition. **b)** Expression profiles of the TCGA-333 primary prostate cancer cohort ($n = 333$ patients) were interrogated for correlation between the ERF mRNA level and two androgen transcriptional activity signatures. P values were calculated by the Spearman correlation test. **c)** The same analysis as **b)** was applied to the SU2C-150 ($n = 150$ patients) metastatic castration-resistant prostate cancer cohort³ (mCRPC).

B. Major Task 2: Evaluation of role of point mutants in ERF tumor

We queried all published prostate cancer genome cohorts ($n = 930$ patients) and compiled a list of all ERF mutations (Fig. 4a), present in 1–3% of patients. The mutations include the specific K401fs and G299fs loss-of-function truncations (initially defined in craniosynostosis families), as well as similar missense mutations in the ETS domain. Mapping of these ETS missense mutations onto the known crystal structure of ERG revealed that the altered residues are located within conserved helices (Fig. 4b), with four of the five conserved mutations predicted to be destabilizing by *in silico* analysis. Expression of complementary DNAs (cDNAs) containing the ETS missense or truncating mutations in LNCaP prostate cancer cells led to reduced ERF steady-state levels relative to wild-type ERF despite robust messenger RNA (mRNA) expression (Fig. 4c, d), in agreement with prior craniosynostosis studies. Collectively, this pointed to ERF point mutations in prostate cancer as being destabilizing.

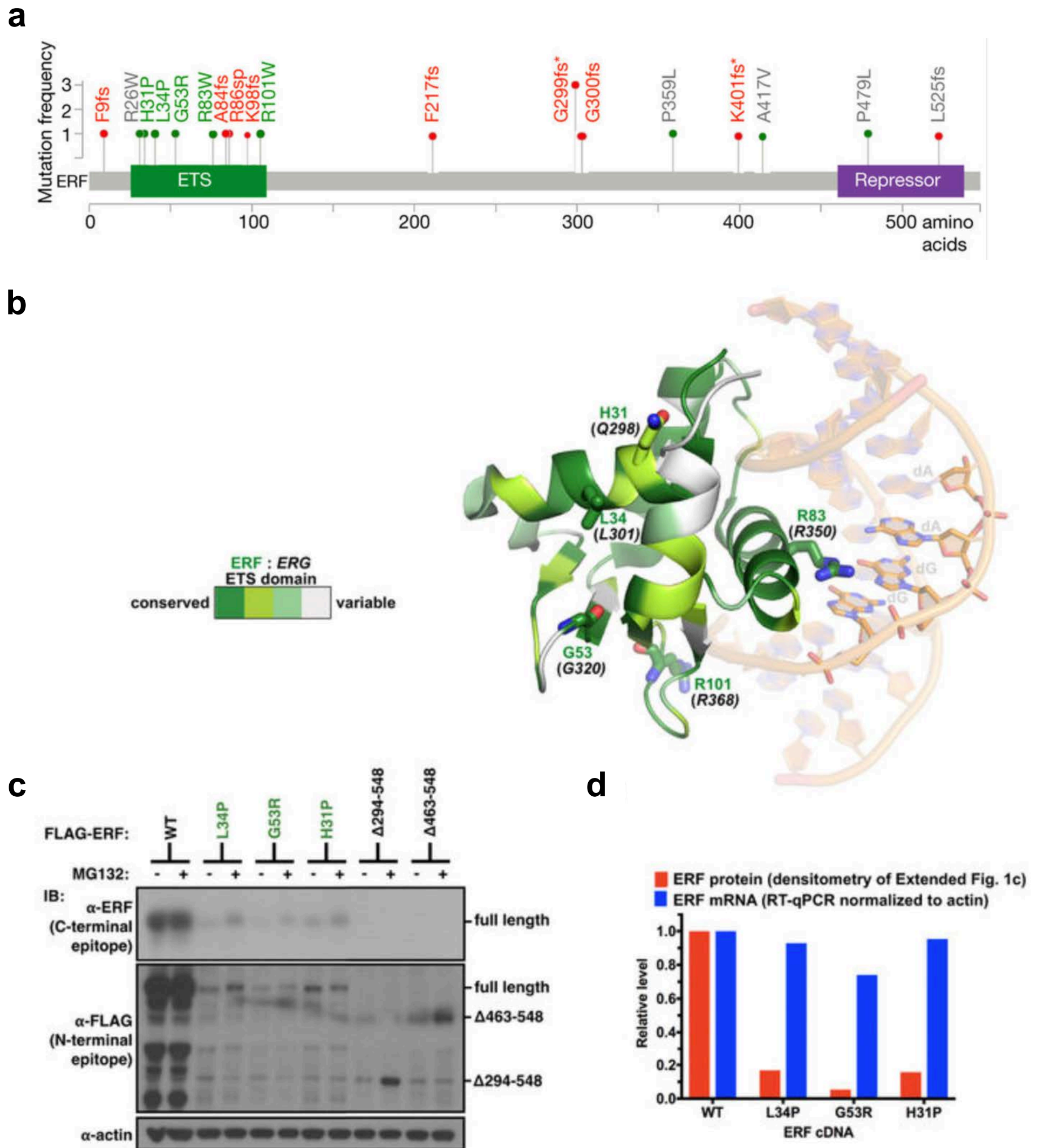


Figure 4 - a) ERF point mutations identified in all prostate cancer cohorts. *Mutations shared with patients having craniosynostosis. Green: ETS missense mutations of residues conserved with ERG. Red: frameshift (fs) / splice-site (sp) mutations upstream of repressor domain. **b)** ERG ETS domain (Protein Data Bank accession number 4IRI) illustrating sequence conservation with ERF. ERF missense mutations indicated by sticks. **c)** Expression of ERF mutant proteins in LNCaP cells. **d)** ERF mutant protein densitometry from immunoblot in c compared with mRNA RT-qPCR.

C. Major Task 3: Evaluation of ability of MEK/ERK inhibitor to augment tumor suppressor activity of ERF

Nothing to report

Specific Aim 3: To interrogate and map how ERF may regulate androgen-mediate transcription via its novel interaction with AR

A. Major Task 1: Determination of role of ERF in AR signaling

The inverse correlation between ERF mRNA level and the androgen receptor signature is also observed in the half of prostate cancers that possess the TMPRSS2-ERG fusion (noted previously in Fig. 3b, c), suggesting that ERF may have an androgen receptor repressive function in this subtype as well. To investigate this possibility, the expression of ERF (Fig. 5a) or ERG was separately inhibited via shRNA in the ERG-fusion-positive VCaP cell line and the androgen transcriptome analyzed, looking for genes with a two-fold change in expression by RNA-seq upon 1nM dihydrotestosterone (DHT) addition, FDR<0.05. Consistent with prior literature, inhibition of ERG expression ('ERG-low') resulted in a contracted androgen transcriptome compared with the wild-type state ('ERG-high') (Fig. 5b - Left panel). Conversely, ERF inhibition ('shERF_2') increased the change in expression of androgen receptor target genes and doubled the size of the androgen transcriptome (Fig. 5b - Left panel). DHT treatment had no effect on ERF mRNA levels (Fig. 5b - Mid panel) and doxycycline alone had no effect on gene expression (Fig. 5b - Right panel). ERF knockdown had no effect on ERG protein level, on androgen receptor protein levels, or on androgen receptor subcellular localization (Fig. 5a). Consistent with data observed in Fig. 2c and Fig. 3b-c, ERF knockdown in VCaP cells led to enrichment of androgen-signaling genes, both noted by GSEA interrogation of the above RNA-seq experiment (Fig. 5c) or by validation RT-qPCR experiments (Fig. 5d). Collectively, ERF serves as an endogenous repressor of AR signaling, both in normal prostate and in prostate cancer cells.

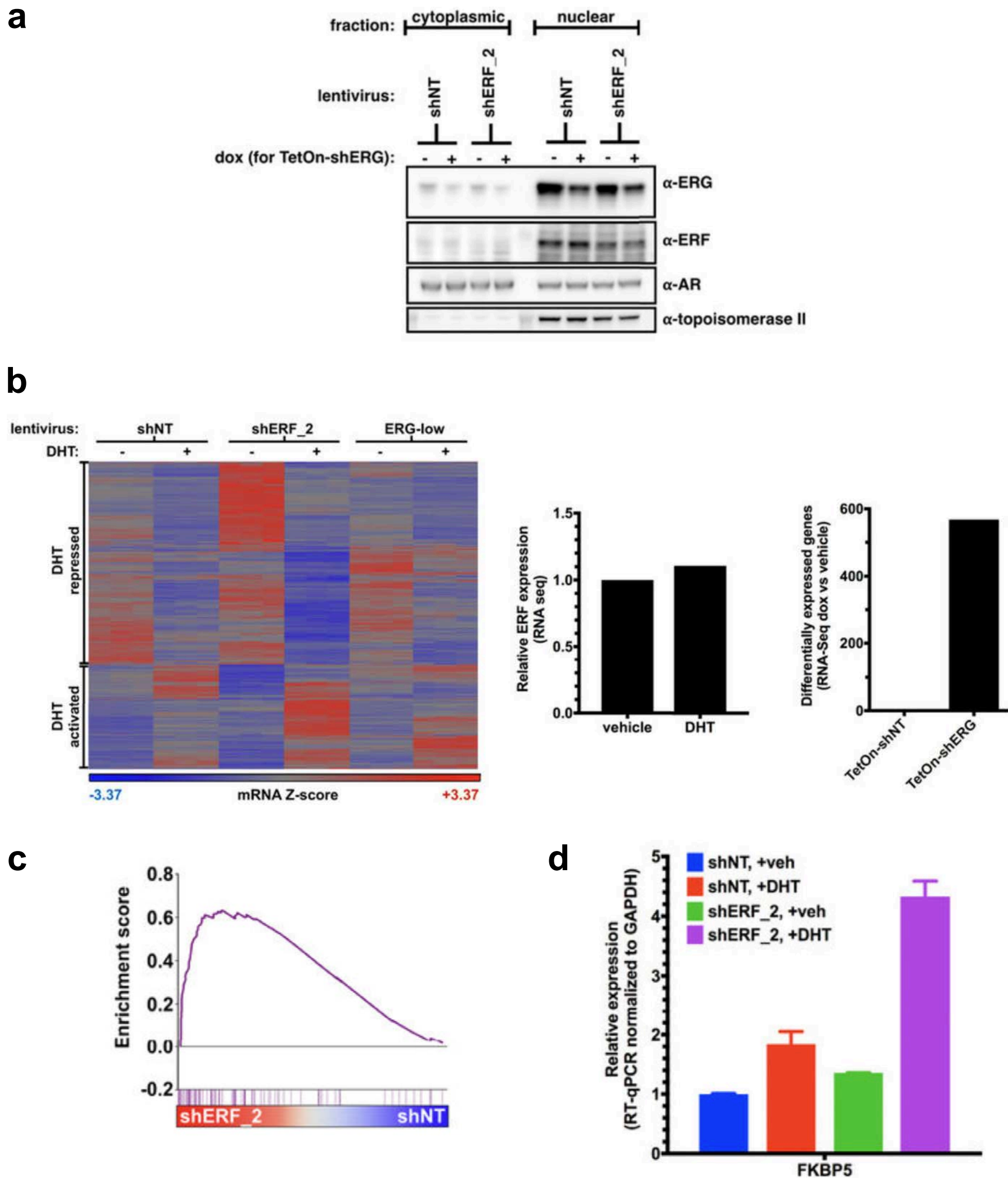


Figure 5 - a) Nuclear/cytoplasmic fractionation of VCaP cells infected with a non-targeting shRNA (shNT) or shRNA targeting ERF (shERF_2). **b)** Left - Androgen-regulated genes (at least a two-fold change, FDR < 0.05 by RNA-seq with 1 nM DHT for 16h) in VCaP cells infected with a doxycycline-inducible shRNA targeting ERG (ERG-low) or targeting ERF (shERF_2) and analysed by heat map; n = 3 biological replicates. Center - Analysis of same RNA-seq data evaluating the effect of dihydrotestosterone (DHT) on ERF expression. Right - Analysis of RNA-seq data to evaluate the effect of doxycycline addition alone. **c)** Interrogation of RNA-seq in shERF_2 VCaP cells (n = 3 biological replicates) by GSEA for Nelson androgen up expression signature. **d)** RT-qPCR of shERF_2-infected VCaP cells treated \pm DHT. Data are mean \pm s.e.m.; n = 3 biological replicates.

- B. Major Task 2: Confirmation of AR-ERF interaction
- C. Major Task 3: Significance of AR-ERF interaction

Nothing to report

Training Opportunities and Professional Development

I have been undergoing an intensive training program for a prospective prostate cancer physician-scientist. I continue to attend bioinformatic seminars necessary for the RNA-seq and ChIP-seq analysis in Aims 1 and 2. I attend oncology grand rounds weekly. I also attend the interdisciplinary bimonthly prostate cancer meeting organized by our Genitourinary Service, and attend the monthly inter-institutional prostate cancer meeting held amongst the prostate cancer-focused labs in New York City. Regarding conferences, I attended the Prostate Cancer Foundation meeting. Dr. Howard Scher continues to provide clinical mentorship regarding my work with patients, and Dr. Charles Sawyers continues to be my mentor with respect to this research project.

Dissemination of Results

The work to date was published (please see 'Products' section).

Next Reporting Period

Aiming to make progress on the clinical information (e.g. prognosis and prediction to therapy response) associated with patients whose tumors possess ERF mutations.

IMPACT

On principal discipline

The findings over the reporting period have furthered our understanding of tumor genetics responsible for prostate cancer progression. Specifically, this project has investigated the poorly understood nature of the ERG fusion-negative tumors and further clarified the nature of the ERG fusion-positive tumors as well. The identification of an ETS factor, ERF, that serves as a tumor suppressor in fusion-negative tumors, but is outcompeted in ERG fusion-positive prostate cancer, is a significant contribution to our understanding of the tumor genetics of prostate cancer.

The results from this proposed research project could also have a major impact on prostate cancer care. Existing treatments for advanced prostate cancer increase survival only on the order of months, and can be associated with significant morbidities. Half of all such cancers lack ERG gene fusions, and at present, we lack a unifying understanding of the key regulators in such tumors. If the project hypothesis is correct, then we may be able to identify a novel treatment strategy for patients possessing fusion-negative tumors. This approach could lead to increased survival and decreased morbidity for men suffering from this disease. In addition to the clinical applications above, this project could shed light on how tumors with and without ERG mutations may actually be similar. This, in turn, would contribute to our understanding of the 50% who do have the ERG mutation, and assist in developing a targeted strategy for them as well.

On other disciplines

Nothing to report

On technology transfer

Nothing to report

Beyond science and technology

Nothing to report

CHANGES/PROBLEMS

Nothing to report

PRODUCTS

Publications, conference papers, and presentations

Publications:

Bose R, Karthaus, WR, Armenia J, Abida W, Iaquina PJ, Zhang Z, Wongvipat J, Wasmuth EV, Shah N, Sullivan PS, Doran MG, Wang P, Patruno A, Zhao Y, International SU2C/PCF Prostate Cancer Dream Team, Zheng D, Schultz N, Sawyers CL. ERF mutations reveal a balance of ETS factors controlling prostate oncogenesis. Nature. 2017 June 29;546(7660):671-5. Published. Federal support was acknowledged.

Presentations:

Bose R, Karthaus W, Armenia J, Abida W, Iaquina P, Wongvipat J, Wasmuth E, Shah N, Doran M, Wang P, Sullivan P, Patruno A, International SU2C/PCF Consortium, Zheng D, Schultz N, Sawyers CS. Loss of function mutations in ETS2 repressor factor, ERF, reveal a balance between positive and negative ETS factors controlling prostate oncogenesis. Prostate Cancer Foundation Annual Scientific Retreat – Carlsbad (2016)

Website(s) or other Internet site(s)

Nothing to report

Technologies or techniques

Nothing to report

Inventions, patent applications, and/or licenses

Nothing to report

Other Products

Nothing to report

PARTICIPANTS & OTHER COLLABORATING ORGANIZATIONS

Individuals

Name: Rohit Bose
Project Role: PI
ORCID ID: 0000-0002-6785-0697
Nearest person month worked: 10.8 months
Contribution to Project: PI, Designed, performed and analyzed experiments.

Change in Other Active Support

Nothing to report

Other Organizations

Nothing to report

SPECIAL REPORTING REQUIREMENTS

None

ERF mutations reveal a balance of ETS factors controlling prostate oncogenesis

Rohit Bose^{1,2}, Wouter R. Karthaus¹, Joshua Armenia^{1,3}, Wassim Abida², Phillip J. Iaquinta¹, Zeda Zhang^{1,4}, John Wongvipat¹, Elizabeth V. Wasmuth¹, Neel Shah^{1,4}, Patrick S. Sullivan¹, Michael G. Doran¹, Ping Wang⁵, Anna Patrino², Yilin Zhao⁵, International SU2C/PCF Prostate Cancer Dream Team*, Deyou Zheng^{5,6,7}, Nikolaus Schultz^{1,3}, & Charles L. Sawyers^{1,8}

Half of all prostate cancers are caused by the *TMPRSS2-ERG* gene fusion, which enables androgens to drive expression of the normally silent E26 transformation-specific (ETS) transcription factor *ERG* in prostate cells^{1,2}. Recent genomic landscape studies of such cancers^{3–8} have reported recurrent point mutations and focal deletions of another ETS member, the ETS2 repressor factor *ERF*⁹. Here we show these *ERF* mutations cause decreased protein stability and mostly occur in tumours without *ERG* upregulation. *ERF* loss recapitulates the morphological and phenotypic features of *ERG* gain in normal mouse prostate cells, including expansion of the androgen receptor transcriptional repertoire, and *ERF* has tumour suppressor activity in the same genetic background of *Pten* loss that yields oncogenic activity by *ERG*. In the more common scenario of *ERG* upregulation, chromatin immunoprecipitation followed by sequencing indicates that *ERG* inhibits the ability of *ERF* to bind DNA at consensus ETS sites both in normal and in cancerous prostate cells. Consistent with a competition model, *ERF* overexpression blocks *ERG*-dependent tumour growth, and *ERF* loss rescues *TMPRSS2-ERG*-positive prostate cancer cells from *ERG* dependency. Collectively, these data provide evidence that the oncogenicity of *ERG* is mediated, in part, by competition with *ERF* and they raise the larger question of whether other gain-of-function oncogenic transcription factors might also inactivate endogenous tumour suppressors.

Recent exome sequencing revealed that 3% of patients in the SU2C-294 metastatic prostate cancer cohort³ (Extended Data Fig. 1a) have somatic point mutations, but not gene fusions, involving the ETS member *ERF*. *ERF* was one of a small number of genes whose mutation frequency and predicted functional impact reached significance by the MutSig algorithm¹⁰. Loss-of-function *ERF* germline mutations and lower *ERF* expression have been previously implicated in the disease complex craniosynostosis¹¹. Notably, the DNA-binding ETS domain of *ERF* is most similar to the *ERG* subfamily¹². However, unlike oncogenic ETS factors¹², *ERF* possesses a transferable carboxy-terminal domain that mediates transcriptional repression⁹.

We queried additional prostate cancer genome cohorts ($n = 930$ patients)^{4–8} (Extended Data Fig. 1a) and found further evidence of *ERF* mutations (Fig. 1a) in 1–3% of patients. The mutations include the specific *K401fs* and *G299fs* loss-of-function truncations also found in craniosynostosis families¹¹, as well as similar missense mutations in the ETS domain. Mapping of these ETS missense mutations onto the known crystal structure of *ERG*¹³ revealed that the altered residues are located within conserved helices (Extended Data Fig. 1b), with four of the five conserved mutations predicted to be destabilizing¹⁴. Expression of complementary DNAs (cDNAs) containing the ETS missense or truncating mutations in LNCaP prostate cancer cells led

to reduced *ERF* steady-state levels relative to wild-type *ERF* despite robust messenger RNA (mRNA) expression (Extended Data Fig. 1c, d), in agreement with the craniosynostosis studies¹¹. In addition, only full-length *ERF* was detected following immunoprecipitation in prostate cancer cells possessing an endogenous heterozygous *K401fs* allele⁵ (Extended Data Fig. 1e). Consistent with destabilization, we were unable to isolate mutant *ERF* ETS domains through recombinant expression in bacteria, whereas appreciable amounts of wild-type *ERF* ETS were obtained (Extended Data Fig. 1f).

In addition to destabilizing mutations, we observed remarkably narrow deletions of the *ERF* locus within the TCGA-333 primary tumour cohort⁴ (Fig. 1b). Median *ERF* expression in those tumours containing focal hemizygous deletions is lower than in normal prostate and diploid *ERF* tumours (Extended Data Fig. 2a, $P = 0.019$). Intriguingly, tumours with either *ERF* mutations or focal deletions are mostly exclusive to *TMPRSS2-ERG*-negative tumours (Fig. 1c, $P = 0.022$). Metastatic tumours in the SU2C-294 cohort³ containing *ERF* point mutations are also mostly exclusive to those without upregulated *ERG*, but this distinction does not reach statistical significance (Extended Data Fig. 2b, $P = 0.066$).

The near complete lack of *ERF* mutations in tumours with *TMPRSS2-ERG* fusions led us to investigate whether *ERF* loss recapitulates the phenotype of *ERG* gain. *ERG* is not expressed in benign prostate epithelium and displays potent oncogenicity in a mouse *Pten*^{−/−} background^{2,15}. On the other hand, *ERF* is endogenously expressed in normal prostate (Extended Data Fig. 2a). To determine whether its loss yields a phenotype similar to *ERG* gain, we infected prostate organoids¹⁶ derived from *Pten*^{+/+} and *Pten*^{−/−} mice¹⁵ with short hairpin RNA (shRNA) targeting mouse *Erf* (shErf_m) (Extended Data Fig. 3a). The *Pten*^{+/+} shErf_m organoids acquired morphological characteristics of *ERG* overexpression¹⁷: they formed single-cell luminal structures lacking basal cells (Fig. 2a), and profiling by RNA sequencing (RNA-seq) demonstrated profound loss of expression of most basal signature genes¹⁸ (Fig. 2b and Extended Data Fig. 2b–d). Consistent with these changes^{17,18}, RNA-seq profiling revealed significant enrichment for genes whose expression is upregulated by androgen in human prostate cancer cells (Extended Data Fig. 2c, e). The *Pten*^{−/−} organoids¹⁶ infected with shErf_m also demonstrated a marked luminal shift (Fig. 2a) and were able to form tumours when grafted back into mice, recapitulating the phenotype of *ERG* overexpression¹⁵ (Fig. 2c).

To assess the impact of *ERF* loss in the half of human prostate cancers that lack *ERG* expression similarly to normal prostate, we infected a human cancer-derived cell line lacking the *TMPRSS2-ERG* gene fusion, CWR22Pc, with shRNA targeting *ERF* (Extended Data Fig. 4a) and analysed its androgen transcriptome. We observed both an increase in

¹Human Oncology and Pathogenesis Program, Memorial Sloan Kettering Cancer Center, 1275 York Avenue, New York, New York 10065, USA. ²Department of Medicine, Memorial Sloan Kettering Cancer Center, 1275 York Avenue, New York, New York 10065, USA. ³Center for Molecular Oncology, Memorial Sloan Kettering Cancer Center, 1275 York Avenue, New York, New York 10065, USA. ⁴Louis V. Gerstner, Jr. Graduate School of Biomedical Sciences, Memorial Sloan Kettering Cancer Center, New York, New York 10065, USA. ⁵Department of Genetics, Albert Einstein College of Medicine, Bronx, New York 10461, USA. ⁶Department of Neurology, Albert Einstein College of Medicine, Bronx, New York 10461, USA. ⁷Department of Neuroscience, Albert Einstein College of Medicine, Bronx, New York 10461, USA. ⁸Howard Hughes Medical Institute, Chevy Chase, Maryland 20185, USA.

*Lists of participants and their affiliations appear at the end of the paper.

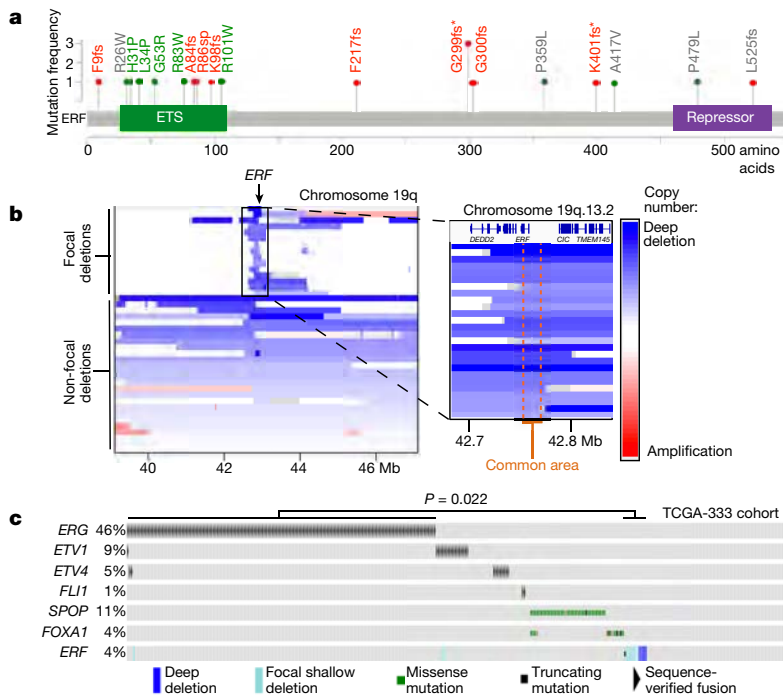


Figure 1 | Recurrent ERF loss-of-function mutations and focal deletions are found in prostate cancer and are mostly exclusive to tumours without TMPRSS2-ERG. **a**, ERF point mutations identified in all prostate cancer cohorts^{3–8}. Green: ETS missense mutations of residues conserved with ERG. Red: frameshift (fs)/splice-site (sp) mutations upstream of repressor domain. **b**, ERF copy number deletions in TCGA-333 human primary prostate cancer cohort⁴. **c**, cBio Oncoprint of patients with primary prostate cancer (n = 333 patients)⁴. Each column corresponds to a unique patient's tumour profile. P value calculated by Fisher's exact two-tailed test.

the number of differentially expressed androgen receptor target genes and in the magnitude of the expression changes (Extended Data Fig. 4b), despite no alteration of androgen receptor mRNA or protein levels (Extended Data Fig. 4a, c). Next, we interrogated the mRNA expression profiles of the primary and metastatic human prostate cohorts TCGA-333 and SU2C-150 (refs 3, 4), respectively. In agreement with our functional studies, *ERF* mRNA levels are inversely correlated with two androgen transcriptional activity signatures^{19,20}, both in normal human prostate and in all primary tumour subtypes (Fig. 2d and

Extended Data Fig. 5a). This reciprocal association is also observed in metastatic cancers if the analysis is limited to tumours without amplification of or mutations in the *AR* gene, which encodes the androgen receptor (Extended Data Fig. 5b). The fact that reduced *ERF* expression enhances androgen receptor transcriptional output even in the absence of mutation or deletion, raises the possibility that *ERF* may have a broader role in prostate oncogenesis.

The inverse correlation between *ERF* mRNA level and the androgen receptor signature is also observed in the half of prostate cancers

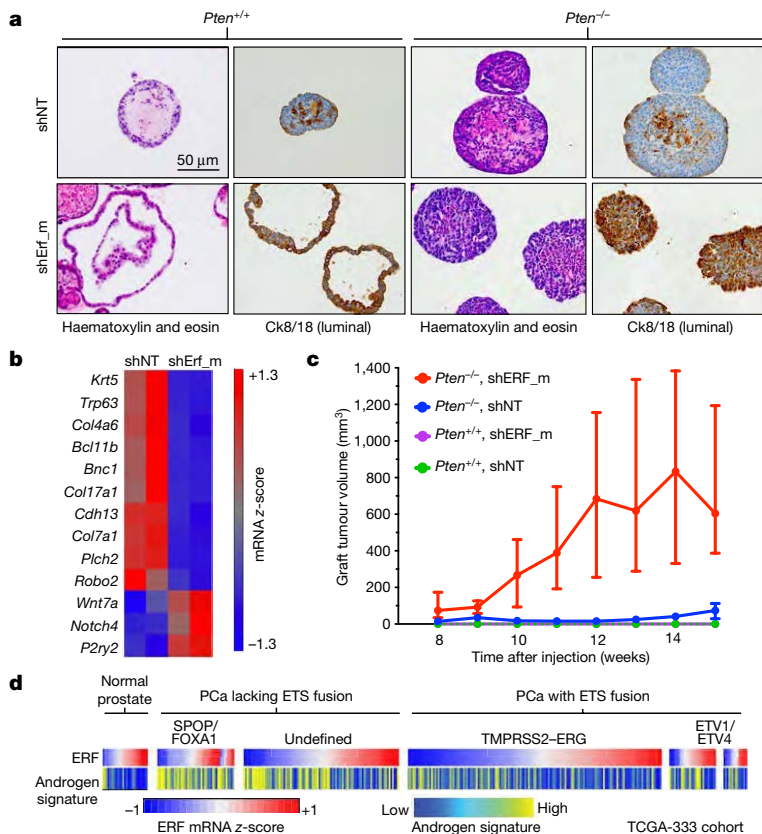


Figure 2 | ERF is a tumour suppressor, a negative regulator of androgen signalling, and its loss phenocopies TMPRSS2-ERG gain. **a**, Immunohistochemistry of mouse prostate organoids infected with non-targeting shRNA (shNT) or targeting ERF (shErf_m). **b**, Basal signature¹⁸ applied to *Pten*^{+/+} organoid RNA-seq (n = 2 biological replicates). **c**, Tumour volumes of organoid grafts. Data are median ± interquartile range; n = 10 tumours per condition. **d**, Human TCGA primary prostate cancer (PCa) cohort⁴ (n = 333 patients) interrogated for ERF mRNA level and the Hieronymus androgen transcriptional activity signature^{4,19,20}.

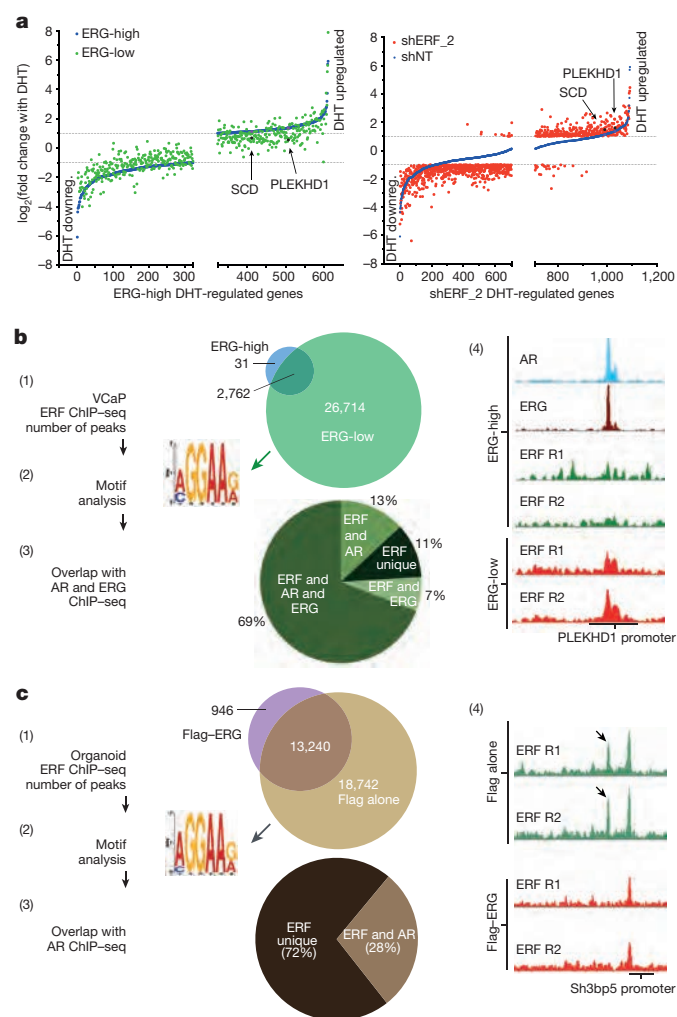


Figure 3 | ERF and TMPRSS2-ERG have opposing effects on the androgen receptor transcriptome and cistrome. **a**, Androgen-regulated genes (as in Extended Data Fig. 4b) analysed by magnitude of change in VCaP cells infected with a doxycycline-inducible shRNA targeting ERG (with doxycycline, ERG-low; without doxycycline, ERG-high) or a constitutive shRNA targeting ERF (shERF_2); $n = 3$ biological replicates. DHT downreg., DHT downregulated. **b**, ERF ChIP-seq in VCaP cells ($n = 2$ biological replicates: R1, R2) analysed by (1) peak overlap, (2) motif analysis, (3) overlap with ERG and androgen receptor ChIP-seq, and (4) example ChIP-seq signals. **c**, ERF ChIP-seq in normal prostate organoids infected with either a Flag-ERG lentivirus or Flag alone, both treated with doxycycline ($n = 2$ biological replicates: R1, R2) and analysed as in **b**.

that possess the *TMPRSS2-ERG* fusion (Fig. 2d), suggesting that ERF may have an androgen receptor repressive function in this subtype as well. To investigate this possibility, the expression of *ERG* or *ERF* was separately inhibited via shRNA (Extended Data Fig. 6a, b) in the ERG-fusion-positive VCaP cell line and the androgen transcriptome analysed as before. Consistent with earlier work¹⁵, inhibition of *ERG* expression ('ERG-low') resulted in a contracted androgen transcriptome compared with the wild-type state ('ERG-high'). Conversely, *ERF* inhibition increased the change in expression of androgen receptor target genes and doubled the size of the androgen transcriptome (Fig. 3a and Extended Data Fig. 7). *ERF* and *ERG* knockdown had no effect on each other's expression, on androgen receptor protein levels, or on androgen receptor subcellular localization (Extended Data Fig. 6c, d).

Given the similarity of their ETS domains¹² (Extended Data Fig. 1b), we postulated that the opposing effects of ERF and ERG on androgen signalling could be explained by competition for androgen-receptor-associated ETS binding sites, which we investigated by ERF chromatin

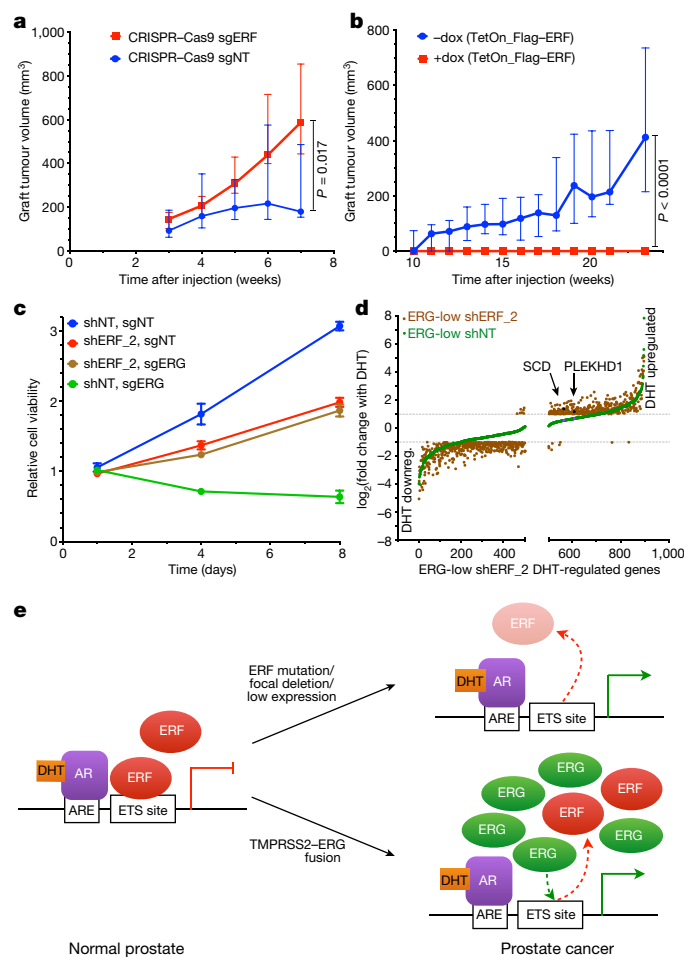


Figure 4 | TMPRSS2-ERG activity is mediated, in part, by inactivation of ERF function. **a**, Tumour volumes of grafts derived from *Pten*^{-/-};R26^{ERG/ERG} organoids infected with CRISPR-Cas9 targeting ERF (sgERF). Data are median \pm interquartile range; $n = 10$ tumours per condition, P value via Mann-Whitney exact two-tailed test. **b**, Similar to **a** but infected instead with doxycycline-inducible Flag-ERF. **c**, Cell viability assay in pooled VCaP cells infected first with shRNA targeting ERF (shERF_2) followed by sgERF. Data are mean \pm s.e.m.; $n = 3$ biological replicates. **d**, Androgen-regulated genes (as in Extended Data Fig. 4b) in ERG-low VCaPs and shERF_2 analysed by magnitude of change; $n = 3$ biological replicates. DHT downreg., DHT downregulated. **e**, ERF inactivation model for genes with androgen receptor and ETS binding sites.

immunoprecipitation followed by sequencing (ChIP-seq) in the ERG-high and ERG-low states (Fig. 3b and Extended Data Fig. 8). *De novo* motif analysis identified the canonical ETS motif as the primary ERF binding site, with 2,793 binding sites in the ERG-high condition ((1) and (2) in Fig. 3b). Remarkably, an additional 26,714 ERF binding sites were observed in the ERG-low state, 76% of which were bound by ERG before ERG knockdown ((1) and (3) in Fig. 3b, and Extended Data Fig. 8d). Furthermore, the ChIP-seq signal intensity of the smaller number of ERF peaks observed in the ERG-high state was increased in the ERG-low state in almost all cases (Extended Data Fig. 8c, e). Finally, ERF peaks in the ERG-low state largely overlap with androgen receptor binding peaks ((3) in Fig. 3b), as previously reported for ERG¹⁵, and are exemplified by *PLEKHD1* and *SCD*²⁰ ((4) in Fig. 3b, and Extended Data Fig. 8f). In the ERG-high state, both genes have prominent androgen-receptor- and ERG-associated binding but only limited ERF binding. However, in the ERG-low state, ERF binding is substantially increased in parallel with a decrease in their androgen-induced expression (Fig. 3a).

Given the role that ERF also plays in benign prostate cells, we performed ChIP-seq to confirm that ERF binds ETS sites in the normal prostate organoids (Fig. 3c). Moreover, transient overexpression of ERG led to a significant decrease of ERF chromatin occupancy (Fig. 3c and Extended Data Fig. 9), consistent with the competition for binding also seen in VCaP cancer cells. We explored the overlap between androgen receptor and ERF sites in normal prostate organoids by androgen receptor ChIP-seq and found 28% of the ERF sites overlap with androgen receptor binding sites ((3) in Fig. 3c). This was lower than observed in the ERG-positive VCaP tumour cells, consistent with differences in androgen receptor chromatin occupancy between normal prostate and cancer²¹.

We next asked whether ERF could modulate oncogenicity mediated by ERG expression. First, we used CRISPR-Cas9 (clustered regularly interspaced short palindromic repeats and CRISPR-associated protein 9) to partially delete ERF (sgErf) in pooled mouse *Pten*^{-/-};R26^{ERG/ERG} organoids (Extended Data Fig. 10a), which require ERG to form tumours¹⁵. The sgErf organoids formed tumours more rapidly than those infected with a non-targeting CRISPR (Fig. 4a). Likewise, induction of human ERF expression in these cells blocked androgen-dependent gene expression (Extended Data Fig. 10b, c) and prevented tumour formation (Fig. 4b). To address the role of ERF in transformation of human prostate cancer cells, we predicted that the anti-proliferative effect of ERG knockdown in ERG-positive cells²² should be rescued by concurrent knockdown of ERF. Consistent with previous findings²², partial ERG deletion via CRISPR-Cas9 led to a complete halt of proliferation (Fig. 4c and Extended Data Fig. 10d). Strikingly, stable shRNA knockdown of ERF before partial ERG deletion rescued cells from ERG-dependent proliferation and survival. Moreover, ERF knockdown restored the constricted androgen transcriptome conferred by ERG loss, including restoration of *SCD* and *PLEKHD1* mRNA upregulation (Fig. 4d and Extended Data Fig. 10e).

We propose that loss of ERF activity, either by rare genomic loss-of-function mutations or more commonly by competition with the *TMPRSS2-ERG* oncogenic gene product, leads to activation of the androgen receptor pathway and prostate cancer (Fig. 4e). The consequences of ERF loss and ERG gain have many common functional consequences, including regulation of luminal morphology, expanded activity of androgen receptor, and an ability to form tumours in a *Pten*^{-/-} background. Such similarities are consistent with their mutual exclusivity and the ability of ERF loss to rescue ERG-positive prostate cancer cells from ERG dependency. On the other hand, the fact that ERG translocations are more common than ERF mutant tumours (46% versus 4%, respectively, in the TCGA-333 primary prostate cancer cohort) raises the possibility that ERG has additional gain-of-function activities that favour oncogenic transformation, such as an intrinsic androgen receptor reprogramming activity^{15,21}. A related but unresolved question is whether the oncogenic phenotype of ERF loss is simply due to loss of repression, or to gain-of-function conferred by competition with an unknown endogenous 'positive' ETS factor. Understanding ETS competition has implications also for ETS-driven leukaemias and sarcomas, and perhaps more broadly for other oncogenic transcription factors for which corresponding loss-of-function mutations in cognate repressors might be considered.

Online Content Methods, along with any additional Extended Data display items and Source Data, are available in the online version of the paper; references unique to these sections appear only in the online paper.

Received 14 July 2016; accepted 4 May 2017.

Published online 14 June 2017.

- Tomlins, S. A. *et al.* Recurrent fusion of *TMPRSS2* and ETS transcription factor genes in prostate cancer. *Science* **310**, 644–648 (2005).
- Carver, B. S. *et al.* Aberrant ERG expression cooperates with loss of PTEN to promote cancer progression in the prostate. *Nat. Genet.* **41**, 619–624 (2009).
- Robinson, D. *et al.* Integrative clinical genomics of advanced prostate cancer. *Cell* **161**, 1215–1228 (2015).
- Cancer Genome Atlas Research Network. The molecular taxonomy of primary prostate cancer. *Cell* **163**, 1011–1025 (2015).

- Gao, D. *et al.* Organoid cultures derived from patients with advanced prostate cancer. *Cell* **159**, 176–187 (2014).
- Kumar, A. *et al.* Substantial interindividual and limited intraindividual genomic diversity among tumors from men with metastatic prostate cancer. *Nat. Med.* **22**, 369–378 (2016).
- Beltran, H. *et al.* Divergent clonal evolution of castration-resistant neuroendocrine prostate cancer. *Nat. Med.* **22**, 298–305 (2016).
- International Cancer Genome Consortium. Prostate cancer - adenocarcinoma. *ICGC Cancer Genome Projects* <https://icgc.org/icgc/cgp/70/508/71331> (2016).
- Sgouras, D. N. *et al.* ERF: an ETS domain protein with strong transcriptional repressor activity, can suppress ets-associated tumorigenesis and is regulated by phosphorylation during cell cycle and mitogenic stimulation. *EMBO J.* **14**, 4781–4793 (1995).
- Lawrence, M. S. *et al.* Mutational heterogeneity in cancer and the search for new cancer-associated genes. *Nature* **499**, 214–218 (2013).
- Twigg, S. R. F. *et al.* Reduced dosage of ERF causes complex craniosynostosis in humans and mice and links ERK1/2 signaling to regulation of osteogenesis. *Nat. Genet.* **45**, 308–313 (2013).
- Hollenhorst, P. C., McIntosh, L. P. & Graves, B. J. Genomic and biochemical insights into the specificity of ETS transcription factors. *Annu. Rev. Biochem.* **80**, 437–471 (2011).
- Regan, M. C. *et al.* Structural and dynamic studies of the transcription factor ERG reveal DNA binding is allosterically autoinhibited. *Proc. Natl Acad. Sci. USA* **110**, 13374–13379 (2013).
- Pires, D. E. V., Ascher, D. B. & Blundell, T. L. DUET: a server for predicting effects of mutations on protein stability using an integrated computational approach. *Nucleic Acids Res.* **42**, W314–W319 (2014).
- Chen, Y. *et al.* ETS factors reprogram the androgen receptor cistrome and prime prostate tumorigenesis in response to PTEN loss. *Nat. Med.* **19**, 1023–1029 (2013).
- Kartha, W. R. *et al.* Identification of multipotent luminal progenitor cells in human prostate organoid cultures. *Cell* **159**, 163–175 (2014).
- Klezovitch, O. *et al.* A causal role for ERG in neoplastic transformation of prostate epithelium. *Proc. Natl Acad. Sci. USA* **105**, 2105–2110 (2008).
- Smith, B. A. *et al.* A basal stem cell signature identifies aggressive prostate cancer phenotypes. *Proc. Natl Acad. Sci. USA* **112**, E6544–E6552 (2015).
- Hieronimus, H. *et al.* Gene expression signature-based chemical genomic prediction identifies a novel class of HSP90 pathway modulators. *Cancer Cell* **10**, 321–330 (2006).
- Nelson, P. S. *et al.* The program of androgen-responsive genes in neoplastic prostate epithelium. *Proc. Natl Acad. Sci. USA* **99**, 11890–11895 (2002).
- Pomerantz, M. M. *et al.* The androgen receptor cistrome is extensively reprogrammed in human prostate tumorigenesis. *Nat. Genet.* **47**, 1346–1351 (2015).
- Wang, J. *et al.* Pleiotropic biological activities of alternatively spliced *TMPRSS2/ERG* fusion gene transcripts. *Cancer Res.* **68**, 8516–8524 (2008).

Supplementary Information is available in the online version of the paper.

Acknowledgements We thank A. Heguy, H. Hieronymus, J. Li, Y. Liang, E. Peguero, M. Pirun, N. Socci, P. Watson, A. Viale, Y. Zhang, Memorial Sloan Kettering Cancer Center core facilities, and the members of the Sawyers laboratory for comments. R.B. was supported by an American Society of Clinical Oncology (ASCO) Young Investigator Award, a Department of Defense Physician Training Award, and a Prostate Cancer Foundation Young Investigator Award. W.A. was supported by an ASCO Young Investigator Award and Prostate Cancer Foundation Young Investigator Award. M.G.D. was supported by a Howard Hughes Medical Institute (HHMI) Summer Medical Fellowship. N.Sch. is supported by the Prostate Cancer Foundation. C.L.S. is an investigator of the HHMI and this project was supported by National Institutes of Health grants CA155169, CA19387, CA092629, and CA008748.

Author Contributions R.B. and C.L.S. conceived and oversaw the project, performed data interpretation, and co-wrote the manuscript. R.B., E.V.W., W.A., Z.Z., and P.S.S. performed immunoblots, R.B. and P.S.S. performed RNA analysis, W.R.K., P.J.I. and R.B. performed immunohistochemistry, J.W. performed the mouse grafting, R.B. and A.P. prepared experiments for ChIP-seq, and R.B. performed *in vitro* cell growth assays. W.R.K. made three-dimensional organoid cultures, E.V.W. made bacterially expressed proteins, and R.B., W.R.K., W.A., E.V.W., P.J.I., and M.G.D. cloned plasmid reagents. E.V.W. performed ETS stability analysis, J.A., N.Sch., and R.B. performed analysis of human prostate cancer cohorts, N.Sch. performed gene set enrichment analysis (GSEA), and P.W., Y.Z., and D.Z. performed ChIP-seq analysis. All individual authors made intellectual contributions and reviewed the manuscript. The International SU2C/PCF Cancer Dream provided four unpublished ERF point mutations. The International SU2C-PCF Dream Team is led by A.M.C. and C.L.S.

Author Information Reprints and permissions information is available at www.nature.com/reprints. The authors declare no competing financial interests. Readers are welcome to comment on the online version of the paper. Publisher's note: Springer Nature remains neutral with regard to jurisdictional claims in published maps and institutional affiliations. Correspondence and requests for materials should be addressed to C.L.S. (sawyersc@mskcc.org).

Reviewer Information Nature thanks J. Carroll, T. Sato, L. Trotman and the other anonymous reviewer(s) for their contribution to the peer review of this work.

The International SU2C/PCF Prostate Cancer Dream Team

Dan Robinson^{9,10}, Eliezer M. Van Allen^{11,12}, Yi-Mi Wu^{9,10}, Nikolaus Schultz^{13,14}, Robert J. Lonigro⁹, Juan-Miguel Mosquera^{15,16,17,18}, Bruce Montgomery^{19,20,21}, Mary-Ellen Taplin¹¹, Colin C. Pritchard²², Gerhardt Attard^{23,24}, Himisha Beltran^{16,17,18,25}, Wassim Abida²⁶, Robert K. Bradley¹⁹, Jake Vinson²⁷, Xuhong Cao^{9,28}, Pankaj Vats⁹, Lakshmi P. Kunju^{9,10,29}, Maha Hussain^{29,30,31}, Scott A. Tomlins^{9,10,29,31}, Kathleen A. Cooney^{29,30,31}, David C. Smith^{29,30,31}, Christine Brennan⁹, Javed Siddiqui⁹, Rohit Mehra^{9,10}, Yu Chen^{9,25,26}, Dana E. Rathkopf^{25,26}, Michael J. Morris^{25,26}, Stephen B. Solomon³², Jeremy C. Durack³², Victor E. Reuter³³, Anuradha Gopalan³³, Jianjiong Gao¹⁴, Massimo Loda^{11,12,34,35}, Rosina T. Lis^{11,34}, Michaela Bowden^{11,34,35}, Stephen P. Balk³⁶, Glenn Gaviola³⁷, Carrie Sougnez¹², Manaswi Gupta¹², Evan Y. Yu^{20,21}, Elahe A. Mostaghe^{19,20,21}, Heather H. Cheng^{19,20,21}, Hyojeong Mulcahy³⁸, Lawrence D. True³⁹, Stephen R. Plymate^{20,21}, Heidi Dvinge¹⁹, Roberta Ferraldeschi^{23,24}, Penny Flohr^{23,24}, Susana Miranda^{23,24}, Zafeiris Zafeiriou^{23,24}, Nina Tunariu^{23,24}, Joaquin Mateo^{23,24}, Raquel Perez-Lopez^{23,24}, Francesca Demichelis^{16,40}, Brian D. Robinson^{15,16,17,18}, Marc Schiffman^{15,18,41}, David M. Nanus^{16,17,18,25}, Scott T. Tagawa^{16,17,18,25}, Alexandros Sigaras^{16,42,43}, Kenneth W. Eng^{16,42,43}, Olivier Elemento⁴², Andrea Sboner^{15,16,18,42}, Elisabeth I. Heath^{44,45}, Howard I. Scher^{25,26}, Kenneth J. Pienta⁴⁶, Philip Kantoff³, Johann S. de Bono^{23,24}, Mark A. Rubin^{15,16,17,18}, Peter S. Nelson^{18,20,21,47,48}, Levi A. Garraway^{11,12}, Charles L. Sawyers⁴⁹ & Arul M. Chinnaiyan^{9,10,28,29,31}

⁹Michigan Center for Translational Pathology, University of Michigan Medical School, Ann Arbor, Michigan 48109, USA. ¹⁰Department of Pathology, University of Michigan Medical School, Ann Arbor, Michigan 48109, USA. ¹¹Department of Medical Oncology, Dana-Farber Cancer Institute, Boston, Massachusetts 02215, USA. ¹²Broad Institute of Massachusetts Institute of Technology and Harvard, Cambridge, Massachusetts 02142, USA. ¹³Department of Epidemiology and Biostatistics, Memorial Sloan Kettering Cancer Center, New York, New York 10065, USA. ¹⁴Marie-Josée and Henry R. Kravis Center for Molecular Oncology, Memorial Sloan Kettering Cancer Center, New York, New York 10065, USA. ¹⁵Department of Pathology and Laboratory Medicine, Weill Medical College of Cornell University, New York, New York 10021, USA. ¹⁶Institute for Precision Medicine, Weill Medical College of Cornell University, New York, New York 10021, USA. ¹⁷New York Presbyterian Hospital, New York, New York 10021, USA. ¹⁸Meyer Cancer, Weill Medical College of Cornell University, New York, New York 10021, USA. ¹⁹Computational Biology Program, Public Health Sciences Division and Basic Science Division, Fred Hutchinson Cancer Center, University of Washington, Seattle, Washington 98109, USA. ²⁰Department of Medicine, University of Washington, Seattle, Washington

98109, USA. ²¹Veterans Affairs Puget Sound Health Care System, University of Washington, Seattle, Washington 98109, USA. ²²Department of Laboratory Medicine, University of Washington, Seattle, Washington 98195, USA. ²³The Royal Marsden, Downs Road, Sutton SM2 5PT, UK. ²⁴The Institute of Cancer Research, Downs Road, Sutton SM2 5PT, UK. ²⁵Department of Medicine, Weill Medical College of Cornell University, New York, New York 10021, USA. ²⁶Genitourinary Oncology Service, Department of Medicine, Sidney Kimmel Center for Prostate and Urologic Cancers, Memorial Sloan Kettering Cancer Center, New York, New York 10065, USA. ²⁷Prostate Cancer Clinical Trials Consortium, Memorial Sloan Kettering Cancer Center, New York, New York 10065, USA. ²⁸Howard Hughes Medical Institute, University of Michigan, Ann Arbor, Michigan 48109, USA. ²⁹Comprehensive Cancer Center, University of Michigan Medical School, Ann Arbor, Michigan 48109, USA. ³⁰Department of Internal Medicine, Division of Hematology Oncology, University of Michigan Medical School, Ann Arbor, Michigan 48109, USA. ³¹Department of Urology, University of Michigan Medical School, Ann Arbor, Michigan 48109, USA. ³²Interventional Radiology, Department of Radiology Service, Memorial Sloan Kettering Cancer Center, New York, New York 10065, USA. ³³Department of Pathology, Memorial Sloan Kettering Cancer Center, New York, New York 10065, USA. ³⁴Center for Molecular Oncologic Pathology, Dana-Farber Cancer Institute, Boston, Massachusetts 02215, USA. ³⁵Department of Pathology, Brigham & Women's Hospital, Boston, Massachusetts 02115, USA. ³⁶Division of Hematology-Oncology, Department of Medicine, Beth Israel Deaconess Cancer Center, Beth Israel Deaconess Medical Center, Harvard Medical School, Boston, Massachusetts 02215, USA. ³⁷Department of Musculoskeletal Radiology, Brigham and Women's Hospital, Boston, Massachusetts 02115, USA. ³⁸Department of Radiology, University of Washington, Seattle, Washington 98109, USA. ³⁹Department of Pathology, University of Washington Medical Center, Seattle, Washington 98109, USA. ⁴⁰Laboratory of Computational Oncology, CIBIO, Centre for Integrative Biology, University of Trento, 38123 Mattarello TN, Italy. ⁴¹Division of Interventional Radiology, Department of Radiology, New York-Presbyterian Hospital/Weill Cornell Medical Center, New York, New York 10021, USA. ⁴²Institute for Computational Biomedicine, Department of Physiology and Biophysics, Weill Medical College of Cornell University, New York, New York 10021, USA. ⁴³Department of Physiology & Biophysics, Weill Medical College of Cornell University, New York, New York 10021, USA. ⁴⁴Department of Oncology, Wayne State University School of Medicine, Detroit, Michigan 48201, USA. ⁴⁵Molecular Therapeutics Program, Barbara Ann Karmanos Cancer Institute, Detroit, Michigan 48201, USA. ⁴⁶The James Buchanan Brady Urological Institute and Department of Urology, Johns Hopkins School of Medicine, Baltimore, Maryland 21205, USA. ⁴⁷Division of Human Biology, Fred Hutchinson Cancer Research Center, Seattle, Washington 98109, USA. ⁴⁸Division of Clinical Research, Fred Hutchinson Cancer Research Center, Seattle, Washington 98109, USA. ⁴⁹Howard Hughes Medical Institute, Memorial Sloan Kettering Cancer Center, New York, New York 10065, USA.

METHODS

Cell lines. Mouse prostate organoids were isolated and grown as described previously¹⁶ from the prostates of normal (*Pten*^{+/+}), *Pten*^{-/-}, and *Pten*^{-/-}; *R26*^{ERG/ERG} mice¹⁵. Isolation and growth of MSK-PCa3 cells were described previously⁵. LNCaP cells were obtained from American Type Culture Collection (ATCC) and maintained as previously described²³. CWR22Pc were a gift from M. Nevalainen and maintained as described previously²³. For CWR22Pc cells specifically, charcoal-stripped media was used for transcriptome analysis. VCaP cells were obtained from ATCC (CRL-2876) and maintained as previously described²³. Cells were confirmed to be free of mycoplasma using a Lonza detection kit (LT07-318). Cell line authentication was confirmed by SNP fingerprinting and hallmark gene-fusions/mutations were identified by deep sequencing.

Prostate cancer tumour profiling. Profiles of the various cohorts^{3–7} outlined in Extended Data Fig. 1a can be explored in the cBioPortal for Cancer Genomics (<http://www.cbioportal.org>). The TCGA data can also be accessed through the Broad Institute FireBrowse portal (<http://firebrowse.org/?cohort=PRAD>), and the ICGC–CRUK Prostate Adenocarcinoma data can be accessed through the ICGC Portal (<https://icgc.org/icgc/cgp/70/508/71331>). In Fig. 1a and Extended Data Fig. 2b, we report four previously unpublished mutations in ERF from a larger Stand Up to Cancer³ (SU2C) cohort that will be described in the future.

Organoid histology and xenografts. Organoids were infected with the indicated lentivirus, selected with puromycin and further selected with FACS. For histology and immunohistochemistry, organoids were processed as described previously^{5,16}. Immunohistochemistry was performed using a Ventana BenchMark ULTRA. The anti-CK8/18 antibody was purchased from Abcam (ab53280). *In vivo* xenograft experiments were performed as described previously²³, using 7-week-old male C.B17 SCID mice (Taconic): one million cells were injected into the flank for a total of ten tumours per shRNA and cell type. Once tumours were palpable, tumour volume was measured weekly using a Peira TM900 system (Peira, Belgium). The maximal tumour volume permitted by our Institutional Animal Care and Use Committee under protocol 06-07-012 was 2 cm³, beyond which mice were euthanized. All animal experiments were performed in compliance with the guidelines of the Research Animal Resource Center of Memorial Sloan Kettering Cancer Center.

Inhibition of gene expression, and overexpression. ERF shRNA knockdown experiments were performed by infection and puromycin selection of cells with lentivirus containing the miR-E based *SGEP* or *SGEN* vectors²⁴ guided by J. Zuber containing the following guide sequences: shERF_m: TTGAACCTGTAGGTGAACCGTT, shERF₂: TTGTTTGAATACATCTCCAG, shERF₁: TTGAATTTGAACCTGTAGGTGA, shNT was previously described as Ren.713 targeting *Renilla* luciferase²⁴. ERG shRNA knockdown experiments were performed by infection and neomycin selection of cells with lentivirus containing the *Tet-pLKO*-neo vector gifted by D. Wiederschain (Addgene plasmid 21916) using the previously published ERG shRNA and non-targeting sequences²⁵. For Tet-responsive reporters, either dimethylsulfoxide (DMSO) vehicle or doxycycline (Sigma) was added at 100 ng ml⁻¹. CRISPR–Cas9 experiments were performed by infection and puromycin selection of cells with lentivirus containing the *lentiCRISPRv2* vector gifted by F. Zhang (Addgene plasmid 52961) containing the following guide sequences chosen via the <http://www.genome-engineering.org> website: sgERG (GATAACTCTGCGCTCGTTCG), sgERFm (CCTGCCAAGCGATGACGCC), and previously described sgNT²⁶. Overexpression of cDNAs was achieved by the constitutive or Tet-inducible *pLV*-based lentiviral expression system.

Transcription analysis. RNA was extracted from cell lines using an RNeasy Kit (Qiagen). For quantitative PCR with reverse transcription (RT–qPCR) and RNA-seq experiments, cells were plated in triplicate per condition/infected construct at the beginning of the assay (duplicate for mouse organoid RNA-seq), and thereafter replicates were processed independently. Error bars for bar graphs indicate s.e.m. for the biological replicates. DHT (Sigma) (or DMSO vehicle) was added at 1 nM, and treatments were performed for 16 h. For RT–qPCR, cDNA was generated with a High Capacity cDNA Reverse Transcription Kit (Applied Biosystems). Data were quantified relative to β -actin or GAPDH expression, and relative expression was plotted. Primers for human and mouse ERF were purchased from Qiagen. Other qPCR primers were as follows: androgen receptor (F: CCATCTTGTCGTCAATGTTATGAAGC, R: AGCTTCTGGGTTGTCTCCTCAGTGG), ERG (F: CAAACTCTCCA CGGTTAATGC, R: ACCGGTCCAGGCTGATCT).

For RNA-seq, library preparation and sequencing were performed by the Memorial Sloan Kettering Cancer Center Integrated Genomics Operation Core using Illumina HiSeq with 50 base pair (bp) paired-end reads, with approximately 30 million reads generated for each sample. The output data (FASTQ files) were mapped to the target genome (UCSC HG19 or UCSC MM10) using the rnaStar aligner, which mapped reads genomically and resolved reads across splice junctions.

The 2-pass mapping method was used in which the reads were mapped twice. The first mapping pass used a list of known annotated junctions from Ensembl. Novel junctions found in the first pass were then added to the known junctions and a second mapping pass was done (on the second pass the RemoveNoncanonical flag was used). After mapping, we post-processed the output SAM files using the PICARD tools to add read groups, with AddOrReplaceReadGroups, which sorted the file and converted it to the compressed BAM format. We then computed the expression count matrix from the mapped reads using HTSeq (<http://www-huber.embl.de/users/anders/HTSeq>). The raw count matrix generated by HTSeq was then processed using the R/Bioconductor package DESeq (<http://www-huber.embl.de/users/anders/DESeq/>), which was used both to normalize the full dataset and to analyse differential expression between sample groups. Androgen-regulated genes were defined as a twofold difference, false discovery rate (FDR) < 0.05 with 1 nM DHT treatment for 16 h DHT. For GSEA, statistical analysis was performed with publicly available software from the Broad Institute (<http://www.broadinstitute.org/gsea/index.jsp>).

ChIP. Chromatin processing, as well as anti-androgen receptor, anti-ERG, and immunoglobulin-G ChIP were described previously¹⁵. ERF ChIP was performed with anti-ERF antibody (Pierce PA5-30237). For ChIP–qPCR, the ETS2 promoter primers (forward: TTAATTCCTCCAGAGACTGACGA; reverse: CGCCGCCAGAGACGAT) were used. The PSA upstream sequence lacking the ERF motif or androgen receptor binding motif was described previously²⁷. For ChIP–seq, library preparation and RNA-seq were performed by the Memorial Sloan Kettering Cancer Center Integrated Genomics Operation Core using Illumina HiSeq with 50-bp paired-end reads. The reads were aligned to the human genome (hg19, build 37) or the mouse genome (mm10, build 38) using the program BWA (default parameters) within the PEMapper. The software MACS2 (ref. 28) (–q 0.1) was used for peak identification with data from ChIP input DNAs as controls. Peaks of sizes >100 bp and with at least one base pair covered by >15 reads were selected as the final peaks. Peaks from different conditions were merged to obtain non-overlapping genomic regions, which were then used to determine conditional specific binding. Overlapped peaks were defined as those sharing at least one base pair. Two replicates were performed per condition, and peaks called in both replicates were used as the final peaks for each condition. To generate heat maps depicting ERF ChIP–seq read density in ± 2 kilobase regions of the ERF peak summits, the same number of ChIP–seq reads from different conditions were loaded into the software seqMINER²⁹, and the resulting read density matrices were sorted by the read densities in the ERG-low condition in VCaP cells or wild-type condition for the mouse prostate organoids, before colouring. The criteria for assigning peaks to genes have been described previously^{30,31}. The MEME–ChIP software³² was applied to 300-bp sequences around the peak summits for motif discovery.

Immunoprecipitation and western blot analysis. Protein was extracted from cell lines using M-PER Reagent (Thermo Scientific) and quantified by BCA Protein Assay (ThermoFisher Scientific). Nuclear/cytoplasmic fractionation was achieved with an NE-PER kit (ThermoFisher Scientific). ERF immunoprecipitation was performed with anti-ERF antibody (Pierce PA5-30237). Western blots were imaged using the fluorometric-based LiCor system, using primary antibodies against ERF (Santa Cruz sc-15435 or Abcam ab61108) and PTEN (Cell Signaling 9188). Western blotting for androgen receptor, ERG, GAPDH, and actin was described previously¹⁵.

In vitro growth assay. Cells were plated in triplicate and assayed at the time points indicated using CellTiter-Glo (Promega). Viability was plotted normalized to day 1. Error bars indicate s.e.m.

Statistics. Mutual exclusivity in the cBio Oncoprints was calculated using a two-tailed Fisher's exact test. For RT–qPCR and RNA-seq experiments, cells were plated in triplicate per condition/infected construct at the beginning of the assay (duplicate for mouse organoid RNA-seq), and thereafter replicates were processed independently. RT–qPCR bar graphs are plotted as mean \pm s.e.m. For RNA-seq, differentially expressed genes were defined as a twofold difference, FDR < 0.05 of DESeq-normalized expression. For GSEA, statistical analysis was performed with publicly available software from the Broad Institute (<http://www.broadinstitute.org/gsea/index.jsp>). For the correlation of the androgen transcriptional signatures with ERF mRNA in human tumours, statistical significance of correlations was calculated by Spearman's test. Mouse graft experiments consisted of ten tumours per condition, and a Mann–Whitney test was used in Fig. 4 to analyse differences in tumour volume. The sample size estimate was based on our experience with previous experiments^{5,15,23}. No formal randomization process was used to assign mice to a given organoid injection, and experimenters were not blinded.

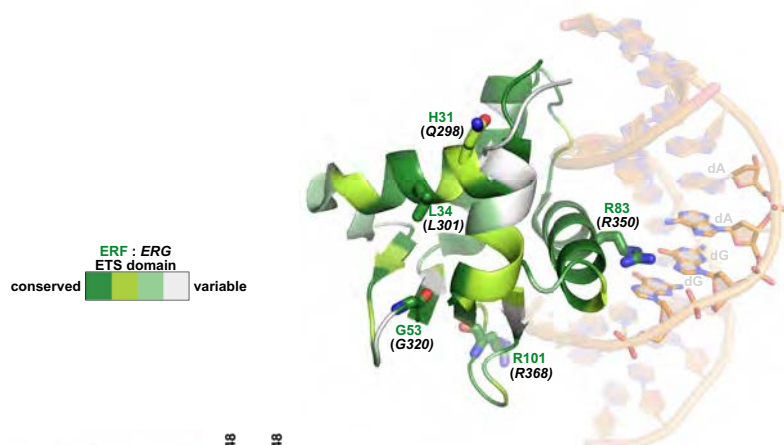
Data availability. All data are available from the authors upon reasonable request. The described RNA-seq and ChIP–seq data have been deposited in the Gene Expression Omnibus under accession number GSE83653.

23. Balbas, M. D. *et al.* Overcoming mutation-based resistance to antiandrogens with rational drug design. *eLife* **2**, e00499 (2013).
24. Fellmann, C. *et al.* An optimized microRNA backbone for effective single-copy RNAi. *Cell Reports* **5**, 1704–1713 (2013).
25. Mounir, Z. *et al.* TMPRSS2:ERG blocks neuroendocrine and luminal cell differentiation to maintain prostate cancer proliferation. *Oncogene* **34**, 3815–3825 (2015).
26. Wang, T., Wei, J. J., Sabatini, D. M. & Lander, E. S. Genetic screens in human cells using the CRISPR–Cas9 system. *Science* **343**, 80–84 (2014).
27. Wang, Q., Carroll, J. S. & Brown, M. Spatial and temporal recruitment of androgen receptor and its coactivators involves chromosomal looping and polymerase tracking. *Mol. Cell* **19**, 631–642 (2005).
28. Feng, J., Liu, T., Qin, B., Zhang, Y. & Liu, X. S. Identifying ChIP–seq enrichment using MACS. *Nat. Protoc.* **7**, 1728–1740 (2012).
29. Ye, T. *et al.* seqMINER: an integrated ChIP–seq data interpretation platform. *Nucleic Acids Res.* **39**, e35 (2011).
30. Arora, V. K. *et al.* Glucocorticoid receptor confers resistance to antiandrogens by bypassing androgen receptor blockade. *Cell* **155**, 1309–1322 (2013).
31. Rockowitz, S. & Zheng, D. Significant expansion of the REST/NRSF cistrome in human versus mouse embryonic stem cells: potential implications for neural development. *Nucleic Acids Res.* **43**, 5730–5743 (2015).
32. Machanick, P. & Bailey, T. L. MEME-ChIP: motif analysis of large DNA datasets. *Bioinformatics* **27**, 1696–1697 (2011).

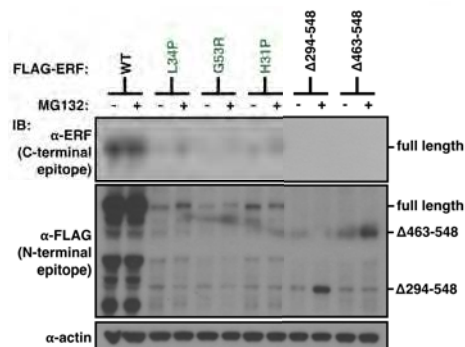
a

Cohorts	Source of specimen	Clinical State	Cohort size	# of patients with ERF point mutations	ERF Point Mutation Rate	Reference	Notes
TCGA-333	Primary site (prostate)	Localized, treatment naive	333	1	0.3%	Cancer Genome Atlas Research Network. The Molecular Taxonomy of Primary Prostate Cancer. Cell 163, 1011–1025 (2015).	
TCGA-498	Primary site	Localized, treatment naive	498	4	0.8%	Broca Institute FireBrowse portal: (http://firebrowse.org/?cohort=PRAD)	Includes TCGA-333
CRUK	Primary site	Mixed	108	1	0.9%	ICGC Portal: https://icgc.org/icgc/cgp/70/508/71331	
SU2C-150	Metastatic site	Castration-resistant, metastatic prostate cancer	150	4	2.7%	Robinson, D. et al. Integrative clinical genomics of advanced prostate cancer. Cell 161, 1215–1228 (2015).	
SU2C-294	Metastatic site	Castration-resistant, metastatic prostate cancer	294	8	2.7%	Pending publication from International SU2C/PCF Consortium.	Includes SU2C-150
FHCRC	Primary or metastatic site	Castration-resistant, metastatic prostate cancer	54	2	3.7%	Kumar, A. et al. Substantial interindividual and limited intraindividual genomic diversity among tumors from men with metastatic prostate cancer. Nature Medicine 1–13 (2016).	
Trento/Cornell/Broad 2016	Metastatic site	Castration-resistant, metastatic prostate cancer	77	1	1.3%	Beltran, H. et al. Divergent clonal evolution of castration-resistant neuroendocrine prostate cancer. Nature Medicine 22, 298–305 (2016).	
MSK Organoids	Local recurrence or metastatic site or circulating tumor cell	Castration-resistant, metastatic prostate cancer	7	1	14.3%	Gao, D. et al. Organoid Cultures Derived from Patients with Advanced Prostate Cancer. Cell (2014).	

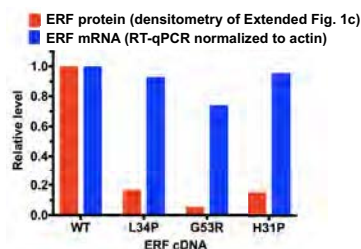
b



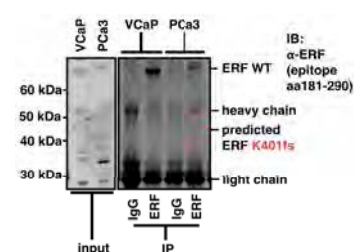
c



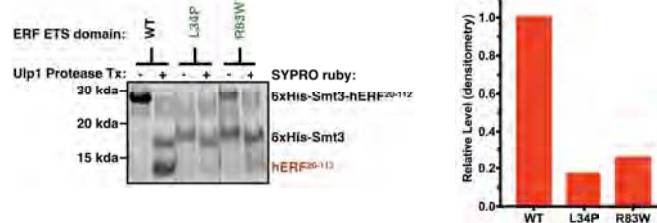
d



e

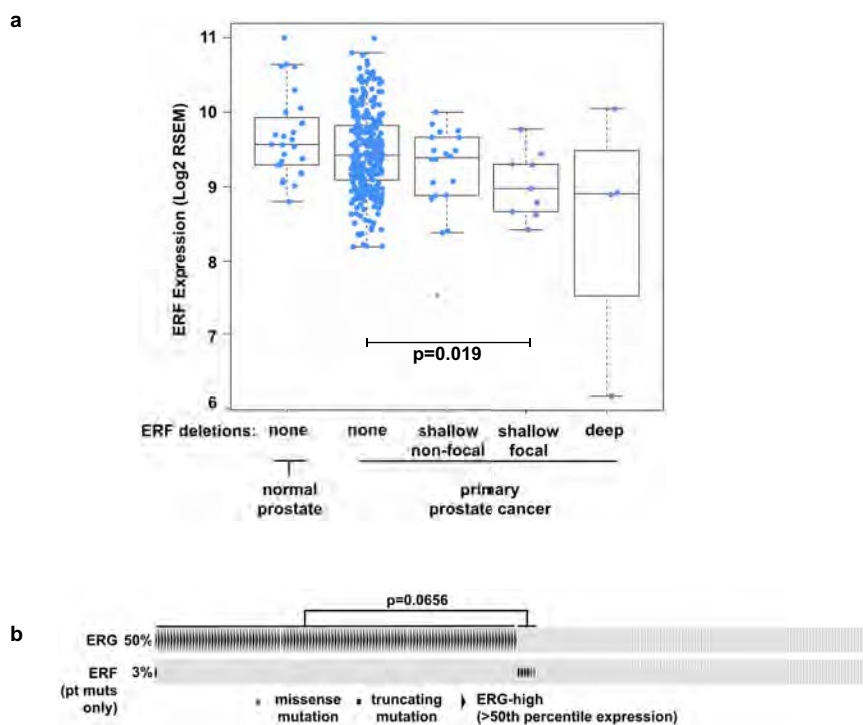


f



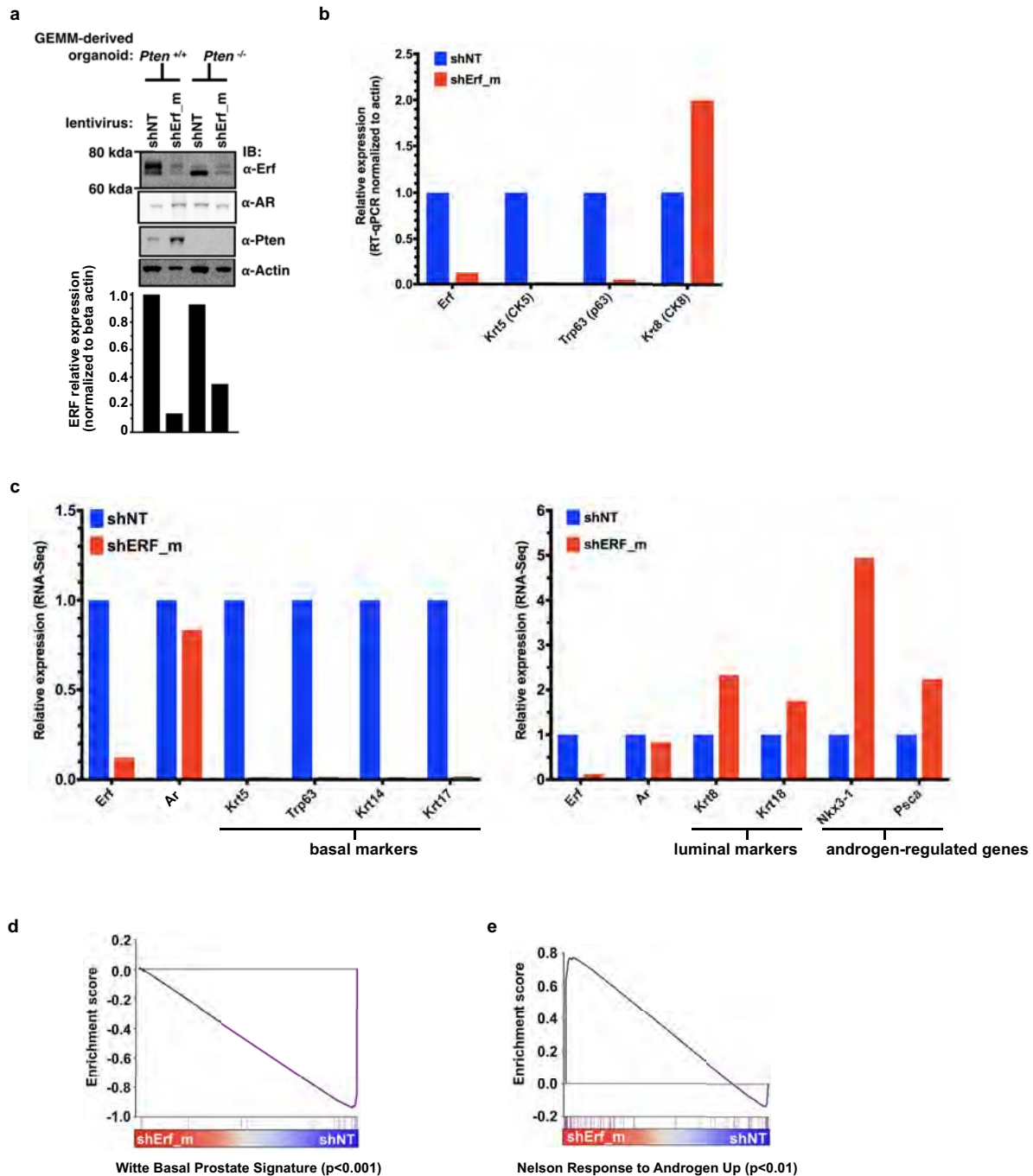
Extended Data Figure 1 | Recurrent ERF loss-of-function mutations are found in prostate cancer and are destabilizing. Related to Fig. 1. **a**, Description of the prostate cancer patient cohorts^{3–8}. **b**, ERF ETS domain (Protein Data Bank accession number 4IRI) illustrating sequence conservation with ERF. ERF missense mutations indicated by sticks. **c**, Expression of ERF mutant proteins in LNCaP cells. For gel source

data, see Supplementary Fig. 1. **d**, ERF mutant protein densitometry from immunoblot in Extended Data Fig. 1c compared with mRNA RT-qPCR. **e**, ERF immunoprecipitation in VCaP and MSK-PCa3 cells. **f**, Left, bacterially expressed ETS domain (hERF^{20–112}) with ERF tumour mutations before (–) or after (+) Ulp1 protease cleavage. Right, densitometry of *in vitro* ETS domains.



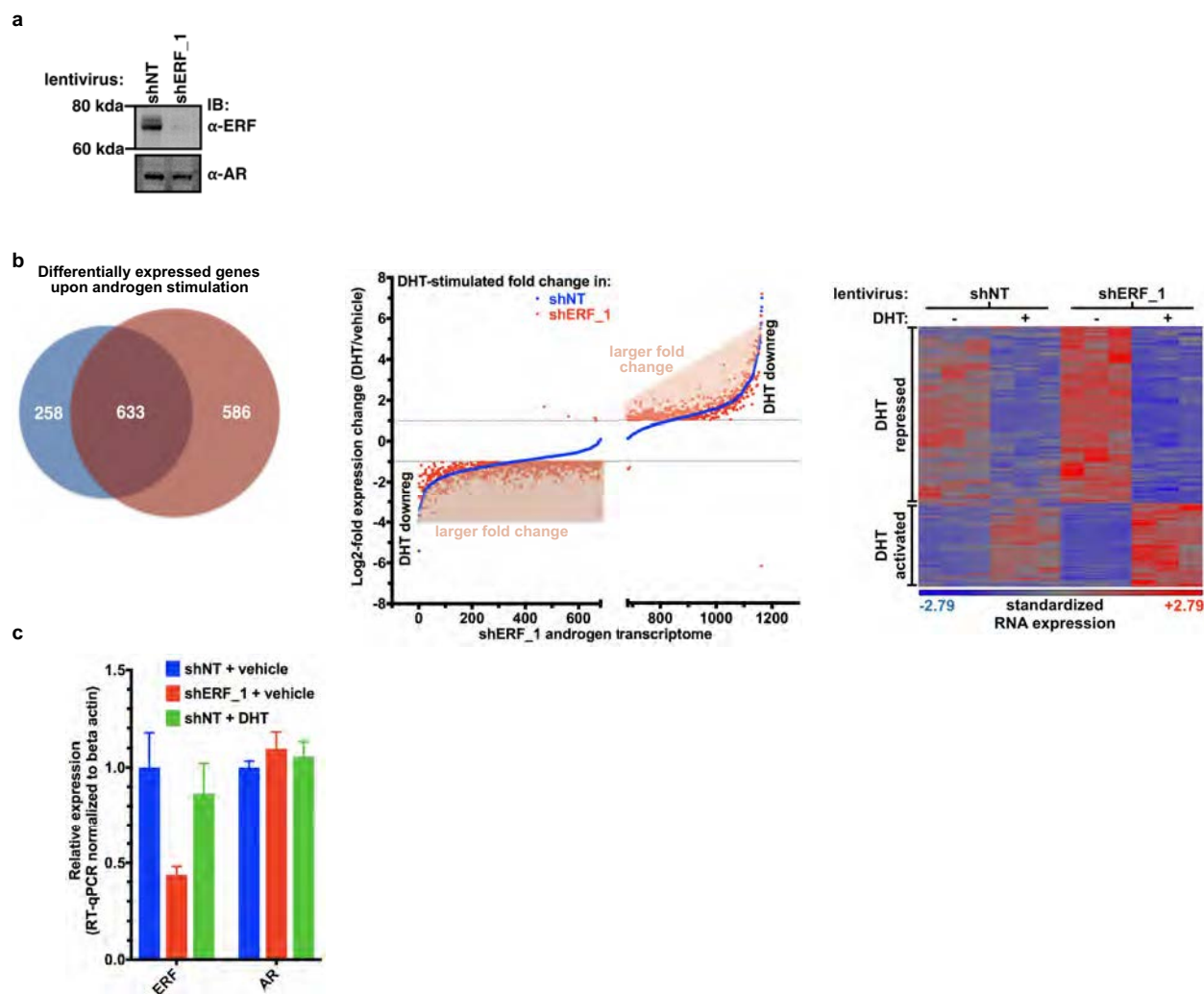
Extended Data Figure 2 | Recurrent ERF loss-of-function mutations and focal deletions are found in prostate cancer and are mostly exclusive to tumours without TMPRSS2-ERG. Related to Fig. 1. **a**, ERF expression in TCGA-333 cohort⁴ ($n = 333$ patients) segregated by copy number loss. Data are Tukey box-and-whisker plots; P value calculated by

two-tailed t -test of $\log_2(\text{RSEM values})$. **b**, cBio Oncoprint of the SU2C-294 ($n = 294$) metastatic prostate cancer cohort³. Unlike Fig. 1c, focal ERF deletions could not be ascertained because of differences between TCGA and SU2C copy number data^{3,4}. P value calculated by Fisher's exact two-tailed test.



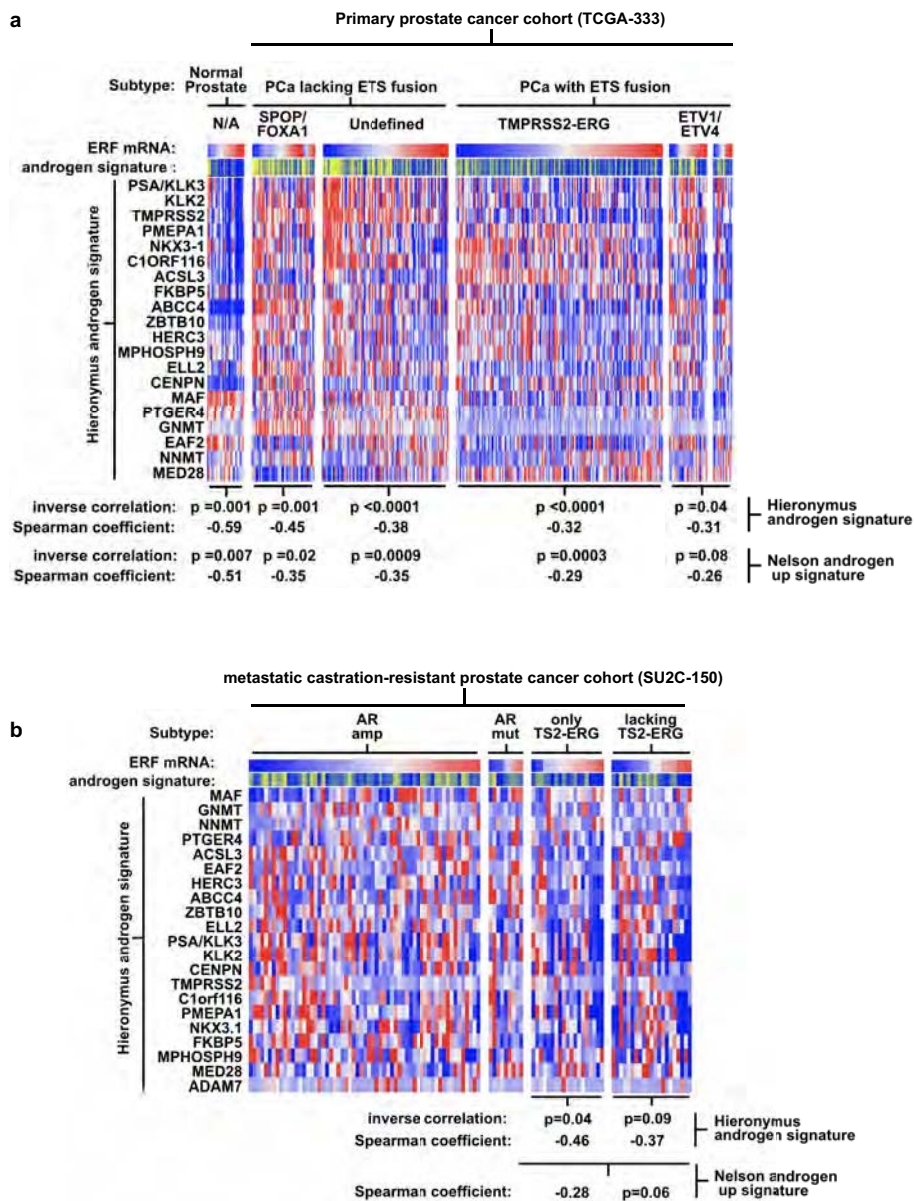
Extended Data Figure 3 | ERF is a negative regulator of androgen signalling. Related to Fig. 2. **a**, Mouse prostate organoids infected with non-targeting shRNA (shNT) or targeting ERF (shErf_m), grown in three-dimensional culture. For RT-qPCR, $n = 2$ biological replicates. For gel source data, see Supplementary Fig. 1. **b**, RT-qPCR analysis of the *Pten*^{+/+} organoids; $n = 2$ biological replicates. **c**, RNA-seq analysis of organoids

derived from *Pten*^{+/+} and *Pten*^{-/-} mouse prostates infected with non-targeting shNT or shErf_m; $n = 2$ biological replicates. **d**, *Pten*^{+/+} organoid RNA-seq ($n = 2$ biological replicates) interrogated by GSEA for expression signature of Witte basal prostate cancer¹⁸. **e**, Same data interrogated by GSEA for Nelson androgen up expression signature²⁰.



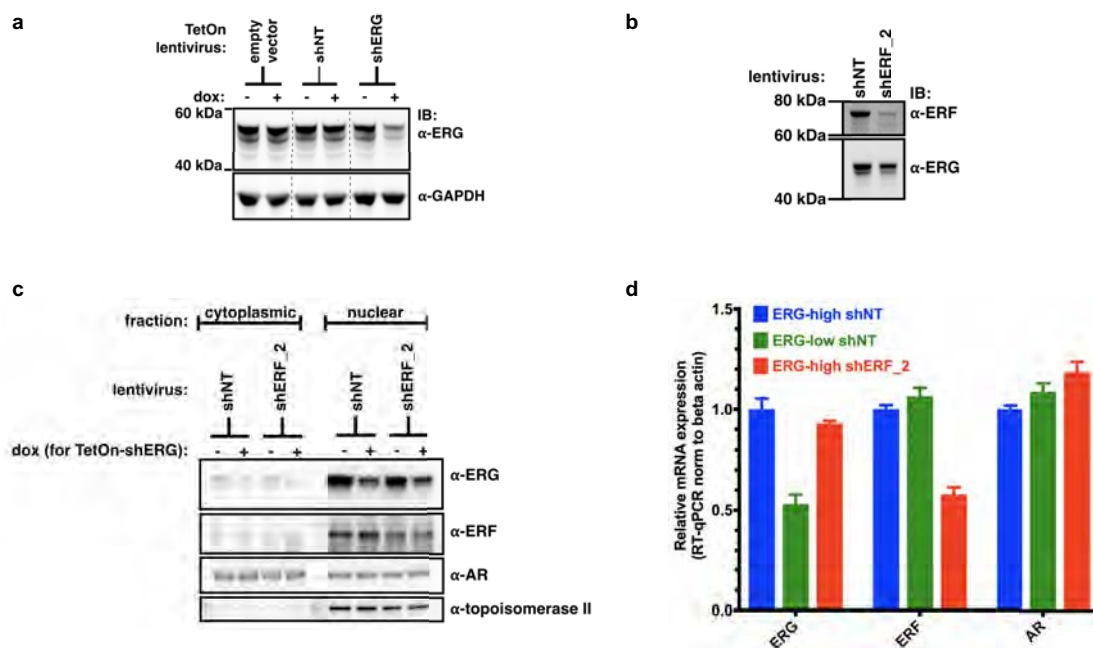
Extended Data Figure 4 | ERF is a negative regulator of androgen signalling. Related to Fig. 2. **a**, CWR22Pc cells infected with shRNA targeting human ERF (shERF_1) or a non-targeting shRNA (shNT). For gel source data, see Supplementary Fig. 1. **b**, Androgen-regulated genes (at least a twofold change, FDR < 0.05 by RNA-seq with 1 nM DHT

for 16h) in CWR22PC cells infected with either shERF_1 or shNT, analysed by the number (left, Venn diagram), the magnitude of expression change (centre, graph), and heat map (right); $n = 3$ biological replicates. **c**, RT-qPCR from CWR22Pc cells infected with shERF_1 or shNT. Data are mean \pm s.e.m.; $n = 3$ biological replicates.



Extended Data Figure 5 | ERF is a negative regulator of androgen signalling. Related to Fig. 2. **a**, Full version of Fig. 2d. Expression profiles of the TCGA-333 primary prostate cancer cohort⁴ ($n = 333$ patients) were interrogated for correlation between the ERF mRNA level and two

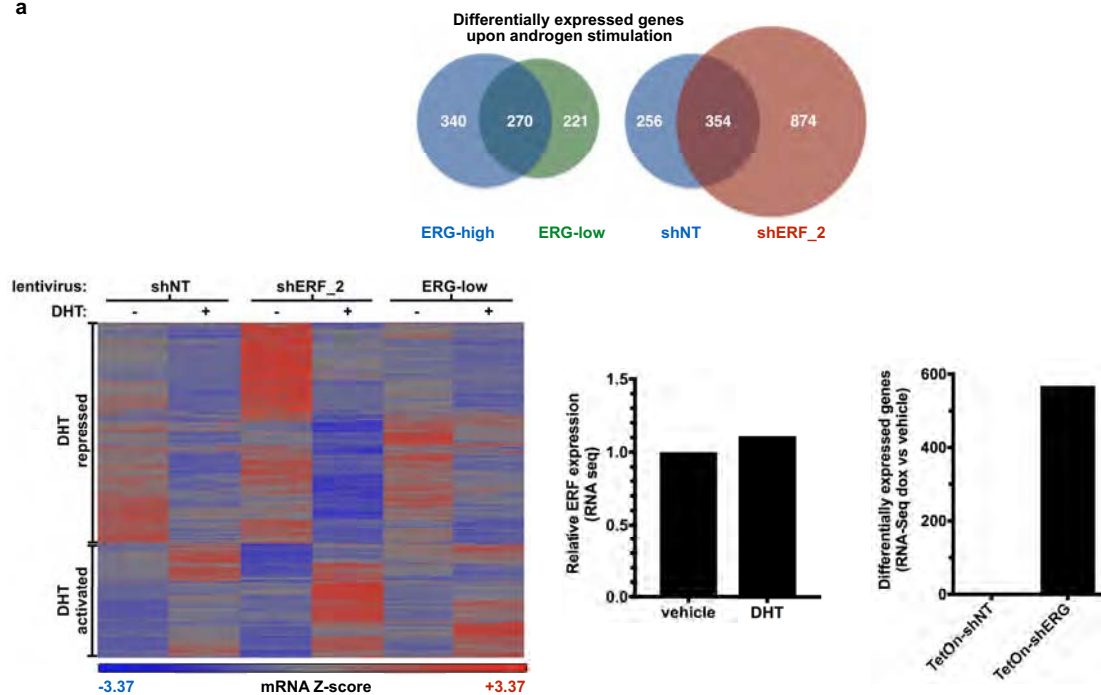
androgen transcriptional activity signatures^{4,19}. P values were calculated by the Spearman correlation test. **b**, The same analysis as **a** was applied to the SU2C-150 ($n = 150$ patients) metastatic castration-resistant prostate cancer cohort³ (mCRPC).



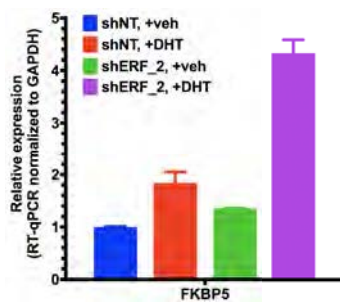
Extended Data Figure 6 | ERF and ERG knockdown do not affect androgen receptor levels or its subcellular localization. Related to Fig. 3. **a**, VCaP cells infected with doxycycline (dox)-inducible shRNA targeting ERG (+dox, ERG-low; –dox, ERG-high). For gel source data, see Supplementary Fig. 1. **b**, VCaP cells infected with shRNA targeting

ERF (shERF_2) or a non-targeting shRNA (shNT). **c**, Nuclear/cytoplasmic fractionation of VCaP cells infected with shNT or shERF_2, and the doxycycline-inducible shRNA targeting ERG (shERG). **d**, RT-qPCR with ERG-low VCaP cells compared with those infected with shERF_2. Data are mean \pm s.e.m.; $n = 3$ biological replicates.

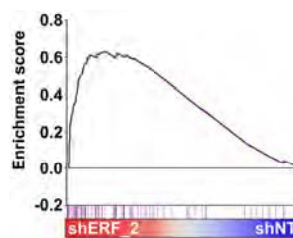
a



b

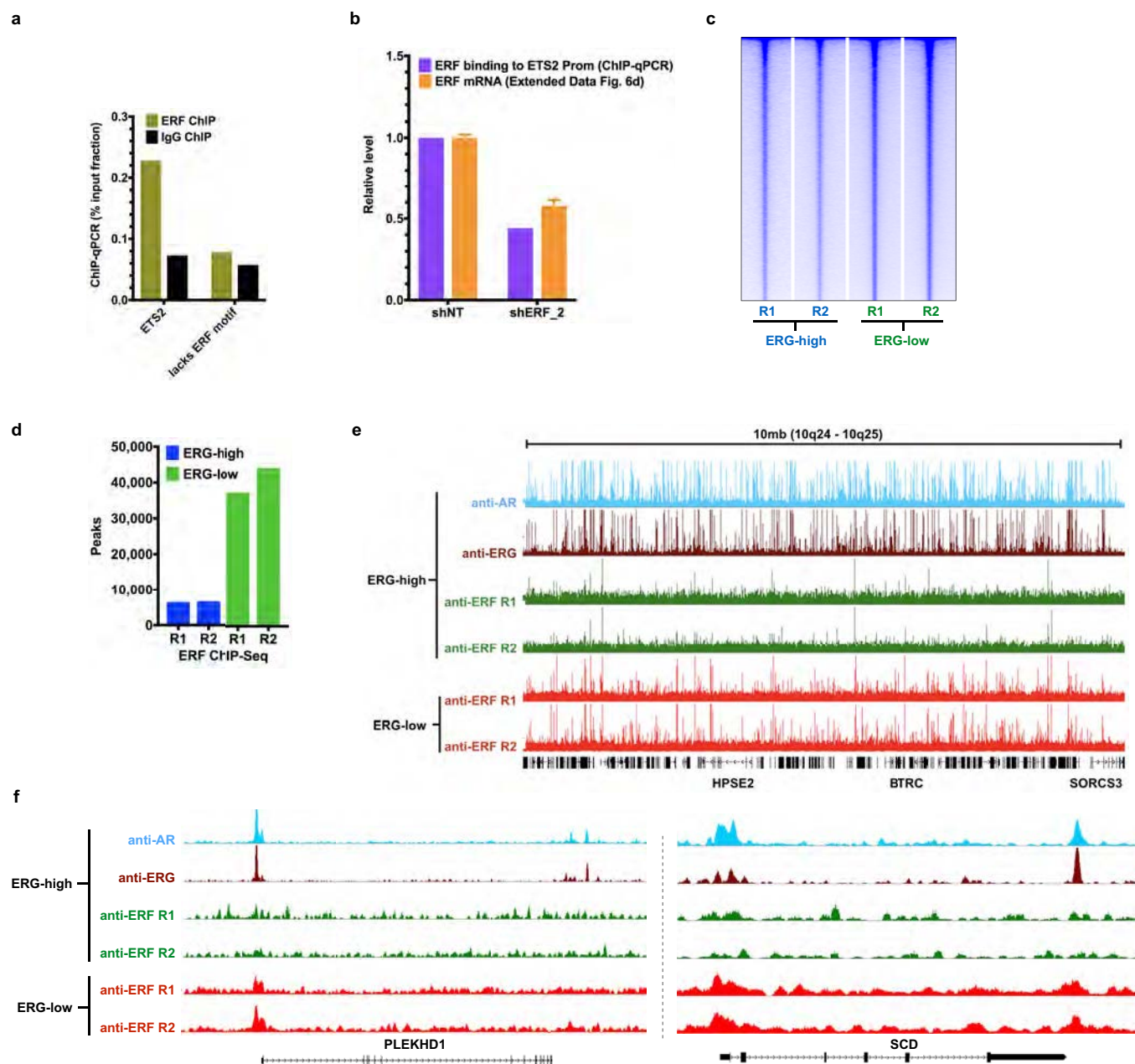


c



Extended Data Figure 7 | ERF and TMPRSS2-ERG have opposing effects on the androgen transcriptome. Related to Fig. 3. **a**, Androgen-regulated genes (at least a twofold change, $FDR < 0.05$ by RNA-seq with 1 nM DHT for 16 h) in VCaP cells infected with a doxycycline-inducible shRNA targeting ERG (with doxycycline, ERG-low; without doxycycline, ERG-high) or a constitutive shRNA targeting ERF (shERF_2) and analysed by number (top) and heat map (bottom left); $n = 3$ biological

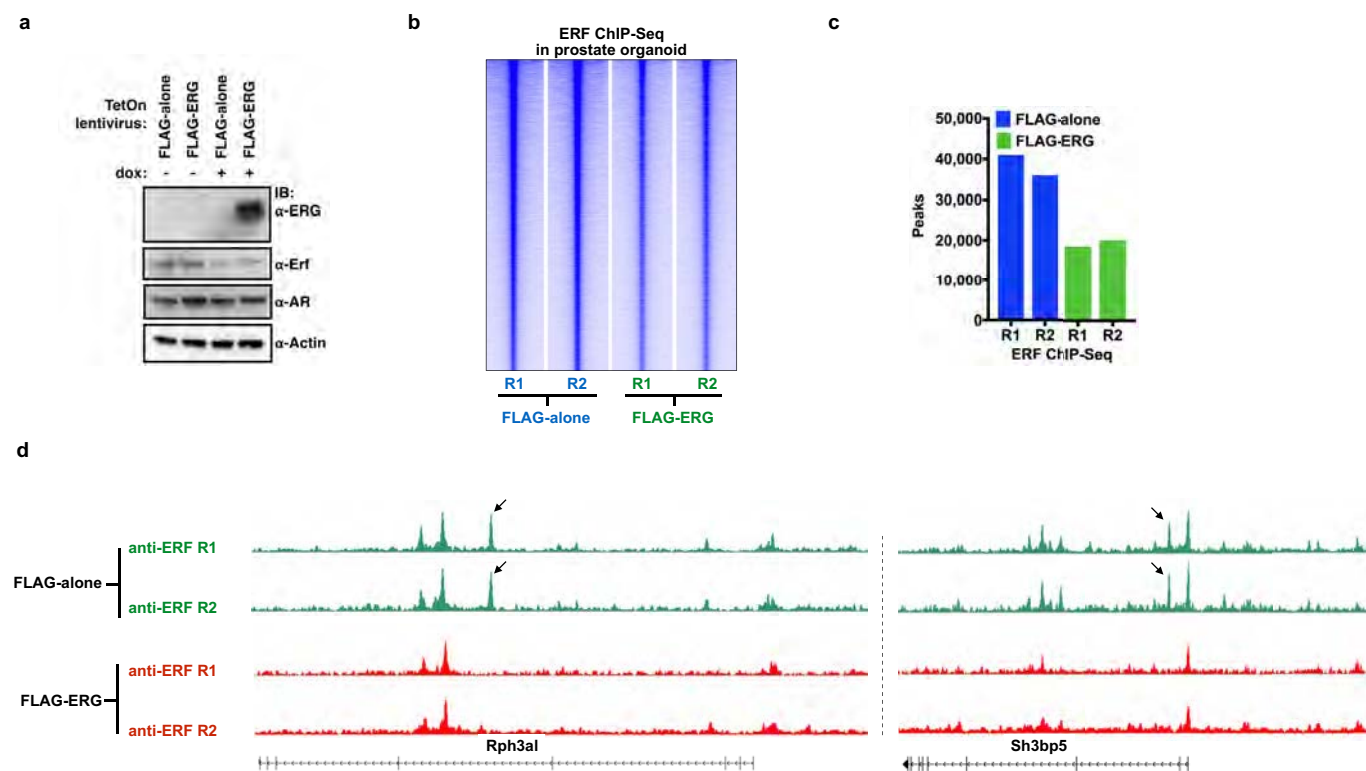
replicates. Bottom centre, RNA-seq analysis evaluating the effect of dihydrotestosterone on ERF expression. Bottom right, the effect of doxycycline alone on RNA-seq differential expression analysis. **b**, RT-qPCR of shERF_2-infected VCaP cells treated \pm DHT. Data are mean \pm s.e.m.; $n = 3$ biological replicates. **c**, Interrogation of RNA-seq in shERF_2 VCaP cells ($n = 3$ biological replicates) by GSEA for Nelson androgen up expression signature²⁰.



Extended Data Figure 8 | ERF and TMPRSS2-ERG have opposing effects on the androgen receptor cistrome. Related to Fig. 3.

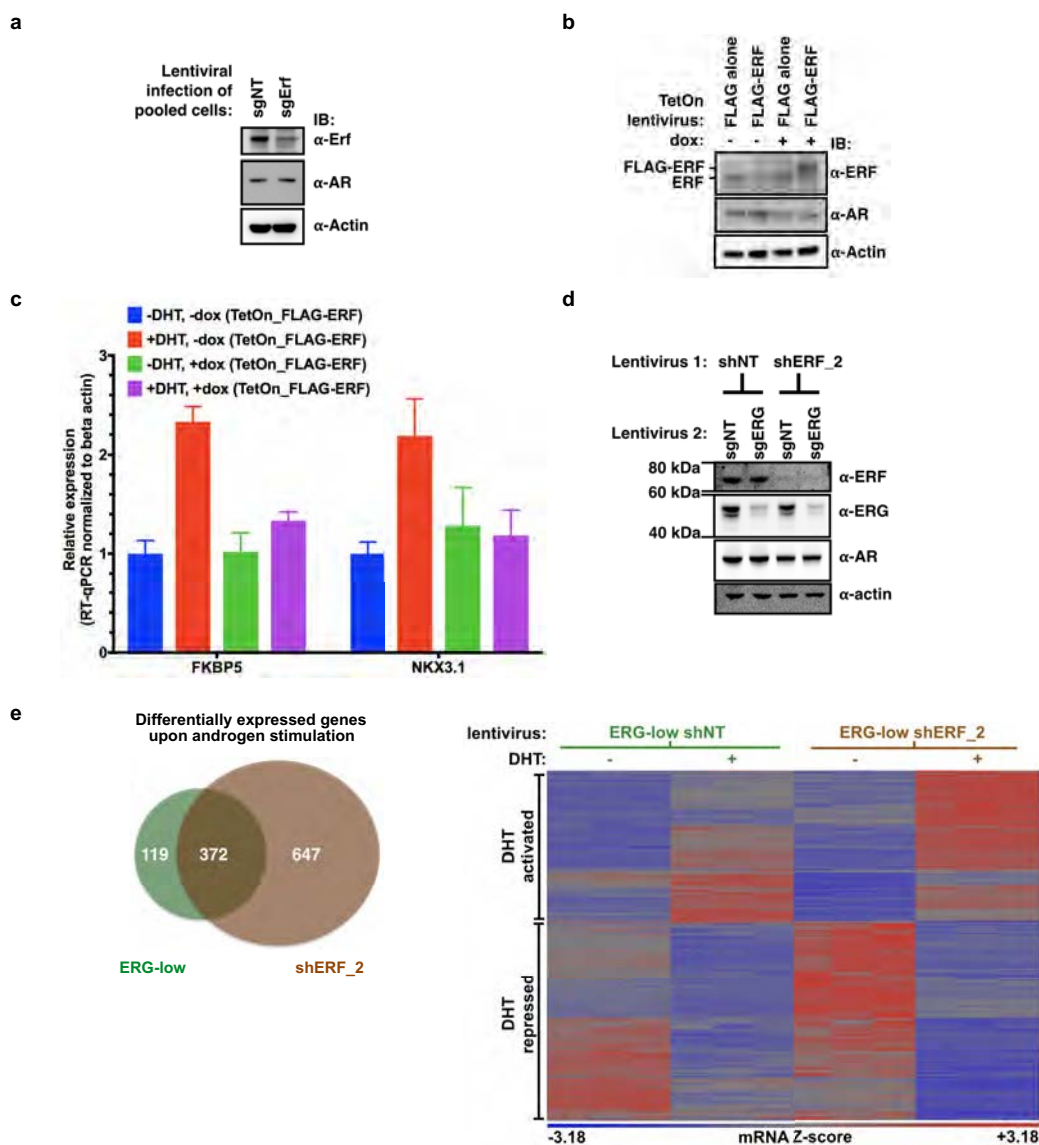
a, ChIP-qPCR ($n = 2$ biological replicates) in VCaP cells, amplifying either the ETS2 promoter region that contains a known ERF binding site⁹, or an upstream element of PSA²⁷ lacking the ERF binding motif noted in (2) in Fig. 3b. **b**, The effect of ERF shRNA knockdown on its binding to the ETS2 promoter as assessed by ChIP-qPCR ($n = 2$ biological replicates), compared with its effect on *ERF* mRNA by RT-qPCR. Data are

mean \pm s.e.m.; $n = 3$ biological replicates. **c**, ERF ChIP-seq in ERG-high or ERG-low ($n = 2$ biological replicates: R1, R2) analysed by heat maps. **d**, Comparison of ERF ChIP-seq peak numbers, $n = 2$ biological replicates: R1, R2. **e**, A 10-Mb region illustrating ChIP-seq of ERF binding in ERG-high condition compared with ERG-low. **f**, ChIP-seq signals for the SCD and PLEKHD1 loci. In both **e** and **f**, ChIP-seq signals at the y axis were normalized by read depths.



Extended Data Figure 9 | ERF expression decreases the ERF cistrome in normal prostate organoids. Related to Fig. 3. **a**, Mouse normal prostate organoids were infected with a TetOn doxycycline-inducible Flag-ERG or empty vector (Flag-alone) and treated with or without doxycycline. For gel source data, see Supplementary Fig. 1. **b**, ERF ChIP-seq in normal prostate

organoids infected with either Flag-alone or Flag-ERG lentivirus, both treated with doxycycline ($n = 2$ biological replicates: R1, R2), and analysed with heat maps. **c**, Comparison of ERF ChIP-seq peak numbers, $n = 2$ biological replicates (R1, R2). **d**, ERF ChIP-seq signals for the Rph3a1 and Sh3bp5 loci, normalized by read depths.



Extended Data Figure 10 | TMPRSS2-ERG activity is mediated, in part, by inactivation of ERF function. Related to Fig. 4. **a**, Pooled mouse *Pten*^{-/-}; *R26*^{ERG/ERG} organoids infected with CRISPR-Cas9 targeting AAVS1 (sgNT) or ERF (sgErf). For gel source data, see Supplementary Fig. 1. **b**, *Pten*^{-/-}; *R26*^{ERG/ERG} organoids infected instead with a doxycycline-inducible Flag-ERF or empty vector (Flag alone). **c**, RT-qPCR of mRNA isolated from the Flag-ERF-infected organoids and treated with or without doxycycline, with or without dihydrotestosterone 1 nM for 16 h. Data are mean \pm s.e.m.; $n = 3$ biological replicates. **d**, Pooled

VCaP cells were first infected with non-targeting shRNA (shNT) or ERF (shERF_2), followed by sgNT or sgERG CRISPR-Cas9. **e**, Androgen-regulated genes (at least a twofold change, FDR < 0.05 by RNA-seq with 1 nM DHT for 16 h) in VCaP cells infected with a doxycycline-inducible shRNA targeting ERG (with doxycycline, ERG-low) and either a constitutive shRNA targeting ERF (shERF_2) or a non-targeting shRNA (shNT). Data analysed by number (left, Venn diagram) and heat map (right); $n = 3$ biological replicates.